HD 28185 revisited: an outer planet, instead of a brown dwarf, on a Saturn-like orbit

Alexander Venner [ORCID],[1]★ Qier An [ORCID],[2,3] Chelsea X. Huang [ORCID],[1] Timothy D. Brandt [ORCID],[2,4] Robert A. Wittenmyer [ORCID][1] and Andrew Vanderburg [ORCID][5]

[1]*Centre for Astrophysics, University of Southern Queensland, Toowoomba, QLD 4350, Australia*
[2]*Department of Physics, University of California Santa Barbara, Santa Barbara, CA 93106, USA*
[3]*Department of Physics and Astronomy, Johns Hopkins University, Baltimore, MD 21218, USA*
[4]*Space Telescope Science Institute, Baltimore, MD 21218, USA*
[5]*Department of Physics and Kavli Institute for Astrophysics and Space Research, Massachusetts Institute of Technology, Cambridge, MA 02139, USA*

ABSTRACT

As exoplanet surveys reach ever-higher sensitivities and durations, planets analogous to the Solar system giant planets are increasingly within reach. HD 28185 is a Sun-like star known to host a $m \sin i = 6$ M_J planet on an Earth-like orbit; more recently, a brown dwarf with a more distant orbit has been claimed. In this work, we present a comprehensive re-analysis of the HD 28185 system, based on 22 yr of radial velocity (RV) observations and precision *Hipparcos–Gaia* astrometry. We confirm the previous characterization of HD 28185 b as a temperate giant planet, with its $385.92^{+0.06}_{-0.07}$ d orbital period giving it an Earth-like incident flux. In contrast, we substantially revise the parameters of HD 28185 c; with a new mass of $m = 6.0 \pm 0.6$ M_J, we reclassify this companion as a super-Jovian planet. HD 28185 c has an orbital period of $24.9^{+1.3}_{-1.1}$ yr, a semimajor axis of $8.50^{+0.29}_{-0.26}$ au, and a modest eccentricity of 0.15 ± 0.04, resulting in one of the most Saturn-like orbits of any known exoplanet. HD 28185 c lies at the current intersection of detection limits for RVs and direct imaging, and highlights how the discovery of giant planets at ≈ 10 au separations is becoming increasingly routine.

Key words: techniques: radial velocities – astrometry – planets and satellites: fundamental parameters – stars: individual: HD 28185.

1 INTRODUCTION

As the search for exoplanets extends into its fourth decade, the population of giant planets at orbital scales comparable to those of the Solar system ($a \gtrsim 5$ au) has come increasingly into focus. Though the most iconic extrasolar giant planets are the short-period hot Jupiters, long-term radial velocity (RV) surveys have shown that giant planets are most frequently found at much more distant separations since at least the work of Cumming et al. (2008). Historically, the frequency of distant planets has been difficult to quantify due to the limited duration of RV surveys, but as observations slowly extend beyond 20–30 yr for many stars it has become increasingly possible to detect giant planets with Jupiter-like and even Saturn-like orbits (e.g. Gregory & Fischer 2010; Rickman et al. 2019). Recent estimates for the occurrence rate of planets more massive than Saturn in the period range $3000 - 10000$ d ($\approx 3 - 10$ au) include $6.9^{+4.2}_{-2.1}$ (Wittenmyer et al. 2020) or $12.6^{+2.6}_{-2.0}$ giant planets per 100 stars (Fulton et al. 2021), demonstrating that these Solar system-like giant planets are not infrequent components of exoplanetary systems. With this increasing clarity, the functional form of the distant giant planet occurrence rate has become a topic of debate; some studies have argued that giant planet occurrence declines beyond $a \gtrsim 3$ au (Fernandes et al. 2019; Fulton et al. 2021), while others propose that the occurrence rate remains approximately constant in the same range (Wittenmyer et al. 2020; Lagrange et al. 2023).

Towards yet wider orbital separations ($\gtrsim 10$ au), direct imaging is providing an increasingly clear picture of giant planet statistics. The most recent results from direct imaging surveys suggest that the occurrence rate of giant planet at separations of at $10 < a < 100$ au is no higher than a few per cent for FGK-type stars (Nielsen et al. 2019; Vigan et al. 2021). This appears to complement the hypothesis of decline in giant planet occurrence towards wider separations (Fulton et al. 2021). However, there remains an area of parameter space at orbital separations of ≈ 10 au where the detection efficiency is low for both RVs and direct imaging. Further discoveries in this intersection of detection limits are therefore important for a complete picture of long-period giant planet occurrence from RVs and direct imaging.

An innovation that has significantly contributed to the study of long-period giant planets in recent years is *Hipparcos–Gaia* astrometry. This is premised on the combination of proper motion data from the *Hipparcos* and *Gaia* missions (Perryman et al. 1997; Gaia Collaboration 2016), allowing for precise measurement of stellar tangential motions across the intervening ~ 25 yr timespan (Brandt 2018; Kervella et al. 2019). In the realm of exoplanet studies, one of the key applications of this data is the characterization of

giant planets discovered through RV surveys. RV planet detections suffer from the well-known $m \sin i$ degeneracy where the mass of the companion depends on the the the orbital inclination i, which cannot be solved from RV data alone. *Hipparcos–Gaia* astrometry has been used to break this degeneracy for a number of long-period RV planets (e.g. Bardalez Gagliuffi et al. 2021; Li et al. 2021; Venner, Pearce & Vanderburg 2022; Philipot et al. 2023a). In some cases, this has shown that the orbits of these companions are viewed near to pole-on, revealing that certain RV planet candidates have masses in the brown dwarf or even stellar regime (Venner, Vanderburg & Pearce 2021). Conversely, even for planets where the astrometric signal is too small to be detected, informative upper limits can be placed on the true mass allowing the companions to be confirmed as planets (Errico et al. 2022).

HD 28185 is a Sun-like star long known to host a $m \sin i = 6 \, M_J$ planet on an Earth-like orbit (Santos et al. 2001). The existence of an additional companion on a wider orbit has also been suspected, and this has recently manifested as a purported brown dwarf (Rosenthal et al. 2021; Feng et al. 2022). In this work, we revisit the HD 28185 system through a comprehensive analysis of published RV data and *Hipparcos–Gaia* astrometry. We significantly revise the parameters of the outer companion in this system, finding that its mass has been substantially overestimated. HD 28185 c is recovered here as a planet of super-Jovian mass, with one of the longest orbital periods of any exoplanet detected (primarily) through RVs. This discovery expands our understanding of giant exoplanets at Solar system-like scales, and highlights how a complete picture of giant planet occurrence rates is increasingly within reach.

2 HISTORY OF STUDY

The $V = 7.8$ mag solar-type star HD 28185 does not have a presence in the astronomical literature prior to the 1990s. The star was first identified as being relatively near to the Sun as a result of the *Hipparcos* mission (Perryman et al. 1997), which measured a stellar parallax of 25.28 ± 1.08 mas. The search for exoplanets was beginning in earnest at this time, and HD 28185 was included as a target for the CORALIE planet search (Udry et al. 2000). Subsequently, Santos et al. (2001) reported the discovery of a planetary companion to this star. They found that HD 28185 b has a minimum mass of $5.7 \, M_J$ and has an orbit with a period of 383 ± 2 d and an eccentricity of 0.07 ± 0.04. Santos et al. (2001) considered the low orbital eccentricity of HD 28185 b to be remarkable as most similar exoplanets known at the time had higher orbital eccentricities, and noted the similarity of the orbit of HD 28185 b with that of Earth. Finally, the authors suggested there is evidence for a longer period RV signal, although they did not provide details.

Though no subsequent publication has re-analysed the CORALIE observations of HD 28185, in the context of a search for stellar companions to exoplanet host stars, Chauvin et al. (2006) mention the existence of an 11 m s^{-1} yr^{-1} RV acceleration of HD 28185 that suggests the existence of a second companion on a wider orbit. The source of this detection is not stated, but it does not originate from Santos et al. (2001). The authors acquired an adaptive optics image of HD 28185 using the Nasmyth Adaptive Optics System (NACO, Lenzen et al. 2003) and did not detect any companions, placing strong limits on any possible outer stellar companions in this system.

After the discovery of HD 28185 b a number of other RV surveys have observed the star. The following studies have published observations of HD 28185:

(i) Minniti et al. (2009) presented an independent detection of HD 28185 b from 3.6 yr of observations with the Magellan Inamori Kyocera Echelle (MIKE) spectrograph at the Magellan II telescope (Bernstein et al. 2003). The authors found a best-fitting period of 379 ± 2 d and eccentricity of 0.05 ± 0.03 for the planet, similar to the results of Santos et al. (2001), and determined a minimum mass of $6.7 \, M_J$. Finally, they noted that no RV acceleration is evident in their data.

(ii) Wittenmyer et al. (2009) observed HD 28185 with the High Resolution Spectrograph (HRS, Tull 1998) at the Hobby-Eberly Telescope for three seasons between 2004–2007 as part of an intensive search for new components in known planet-hosting systems. The authors did not find any evidence for additional planets around the star, particularly on short-period orbits where they were most sensitive. However, they did improve on the parameter precision for HD 28185 b ($P = 385.9 \pm 0.6$ d, $e = 0.092 \pm 0.019$, and $m \sin i = 5.59 \pm 0.33 \, M_J$).

(iii) Butler et al. (2017) published RV observations of HD 28185 spanning $2004 - 2013$ from Keck/HIRES (High Resolution Echelle Spectrometer; Vogt et al. 1994, 2000). As this study was primarily statistical in nature the amount of detail for this system is limited, but an orbital period of $P = 383.72 \pm 0.67$ d and a semi-amplitude of $K = 140.86 \pm 5.05$ m s^{-1} for HD 28185 b are given. Additionally, their adopted model includes a 4.47 ± 1.34 m s^{-1} yr^{-1} RV acceleration, making this the first study to report an RV acceleration after Chauvin et al. (2006).

(iv) Rosenthal et al. (2021) provided an updated analysis of the Keck/HIRES RVs with an extension of the data to 2019. As with Butler et al. (2017), this study is primarily statistical and details are limited, but for HD 28185 b the reported parameters are $a = 1.045^{+0.016}_{-0.018}$ au, $e = 0.0629^{+0.0042}_{-0.0049}$, and $m \sin i = 6.04 \pm 0.2 \, M_J$.

Rosenthal et al. (2021) additionally published the first orbital constraints on the outer companion as observed in the HIRES RVs. They report $a = 15.9^{+7.3}_{-5.1}$ au, $m \sin i = 40^{+43}_{-28} \, M_J$, and $e = 0.26^{+0.12}_{-0.093}$. Based on the nominally high mass of this companion they classified as a brown dwarf; however, as their orbital coverage for this companion is highly incomplete, these parameters are highly uncertain and may not be robust.

Most recently, Feng et al. (2022) have presented a new solution for the HD 28185 system as part of a large-scale joint analysis of RVs and astrometry for a number of systems. Their analysis is based on a selection of published RV data sets (chiefly MIKE and HIRES) plus previously unpublished PFS RVs (Planet Finding Spectrograph; Crane et al. 2010), and astrometry from *Hipparcos* and *Gaia*. Feng et al. (2022) found similar parameters for HD 28185 b as previous works. For the outer companion, which they name as HD 28185 c, they report $P = 17418^{+293}_{-673}$ d $(= 47.7^{+0.8}_{-1.8}$ yr; $a = 13.18^{+0.52}_{-0.69}$ au), $e = 0.120^{+0.021}_{-0.022}$, $i = 57.65^{+8.15}_{-5.75}°$, and $m = 19.64^{+2.27}_{-2.14} \, M_J$. This mass places HD 28185 c well above the canonical deuterium-burning limit at $13 \, M_J$, so this object would conventionally be classified as a brown dwarf.

3 STELLAR PARAMETERS

Owing to its status as a bright and nearby Sun-like star, and perhaps more significantly as a planet host, there is a rich body of study regarding the stellar parameters of HD 28185 (e.g. Santos, Israelian & Mayor 2004; Ghezzi et al. 2010; Ramírez, Meléndez & Asplund 2014; Maldonado et al. 2015; Soto & Jenkins 2018). None the less, for the purposes of completeness we choose to retread this ground in this study.

Table 1. Observed and inferred parameters of HD 28185.

Parameter	Value	Reference
RA α	04:26:26.32	*Gaia* EDR3
Declination δ	-10:33:02.95	*Gaia* EDR3
Parallax ϖ (mas)	25.487 ± 0.021	*Gaia* EDR3
Distance d (pc)	39.20 ± 0.03	Bailer-Jones et al. (2021)
V (mag)	7.81 ± 0.01	Høg et al. (2000)
Spec. T_{eff} (K)	5621 ± 22	Tsantaki et al. (2013)
Spec. $\log g$ (cgs)	4.36 ± 0.05	Tsantaki et al. (2013)
[Fe/H] (dex)	0.19 ± 0.01	Tsantaki et al. (2013)
Model T_{eff} (K)	5602 ± 36	This work
Luminosity ($L_\odot$)	0.970 ± 0.019	This work
M ($M_\odot$)^a	0.974 ± 0.018	This work
R ($R_\odot$)	1.048 ± 0.015	This work
Model $\log g$ (cgs)	4.386 ± 0.015	This work
Age T (Gyr)^a	8.3 ± 1.0	This work

Note.^{a} Includes systematic uncertainties (see the text).

Table 2. Photometry of HD 28185 used in the isochrone fit.

Band	Magnitude (mag)	Reference
B_{T}	8.690 ± 0.016	Høg et al. (2000)
V_{T}	7.891 ± 0.011	Høg et al. (2000)
G	7.6400 ± 0.0028	*Gaia* EDR3
G_{BP}	7.9881 ± 0.0029	*Gaia* EDR3
G_{RP}	7.1235 ± 0.0038	*Gaia* EDR3
J	6.578 ± 0.026	Skrutskie et al. (2006)
H	6.289 ± 0.024	Skrutskie et al. (2006)
K_S	6.185 ± 0.029	Skrutskie et al. (2006)
$W1$	6.164 ± 0.045	Cutri et al. (2012)
$W2$	6.170 ± 0.021	Cutri et al. (2012)
$W3$	6.184 ± 0.015	Cutri et al. (2012)
$W4$	6.095 ± 0.039	Cutri et al. (2012)

HD 28185 is a Sun-like star, with a spectroscopic classification of G5/6V (Houk & Swift 1999) or G6.5V-IV (Gray et al. 2006), at a distance of 39.20 ± 0.03 pc from the Solar system (Bailer-Jones et al. 2021). Its spectroscopic properties have been studied in detail based on data from the High Accuracy Radial velocity Planet Searcher instrument (HARPS; e.g. Sousa et al. 2008; Tsantaki et al. 2013). We list the basic observable properties of the star in Table 1.

To derive the physical parameters of HD 28185, we use the MIST isochrones (Choi et al. 2016; Dotter 2016), constructing a model that uses MINIMINT (Koposov 2021) for isochrone interpolation and EMCEE (Foreman-Mackey et al. 2013) for posterior sampling. The data used for this model consist of photometry from *Tycho*-2 (Høg et al. 2000), *Gaia* EDR3 (Gaia Collaboration 2021), 2MASS (Two Micron All Sky Survey, Skrutskie et al. 2006), and *WISE* (Cutri et al. 2012); these data are reproduced in Table 2. We supplement this with a prior on the distance (from the *Gaia* parallax), and priors on T_{eff} and [Fe/H] from Tsantaki et al. (2013). However, the reported uncertainties on these spectroscopic parameters are strictly internal, and it is known that systematic uncertainties in parameters as found from comparison between different spectrographs may be larger than the nominal uncertainties (e.g. Brewer et al. 2016). We thus conservatively double the widths of the adopted spectroscopic priors (i.e. $T_{\mathrm{eff}} = 5621 \pm 44$ K; [Fe/H] $= 0.19 \pm 0.02$ dex). Due to the close distance of HD 28185, we assume there is no interstellar extinction in the photometry.

Our isochrone model returns a mass $M = 0.974 \pm 0.014$ $M_\odot$ and radius $R = 1.048 \pm 0.015$ $R_\odot$ for HD 28185. The resulting

model $\log g$ of 4.386 ± 0.015 is in excellent agreement with the independent spectroscopic value (4.36 ± 0.05, Tsantaki et al. 2013), supporting the accuracy of these parameters. We find a posterior T_{eff} of 5602 ± 36 K and a subsolar luminosity $L = 0.970 \pm 0.019$ $L_\odot$. The combination of all of these physical parameters leads to an isochronal age $T = 8.3 \pm 0.9$ Gyr.

It is increasingly recognized that the uncertainties on stellar parameters are limited not just by measurement precision, but also by systematic differences between models. To attempt to account for this, we use KIAUHOKU (Tayar et al. 2022) to estimate the model uncertainties on the stellar mass and age. kiauhoku calculates the difference in physical parameters between four stellar models (MIST, Yale/YREC, Dartmouth, and Garching/GARSTEC) when assuming the same observables. For this exercise, we use our values of T_{eff}, $\log g$, and [Fe/H] as input variables. kiauhoku returns large uncertainty terms of $\sigma_M = 0.018$ $M_\odot$ and $\sigma_T = 1.6$ Gyr. However, this is largely driven by the discrepant YREC parameters ($\Delta M_{\mathrm{YREC}} = -0.030$ $M_\odot$ and $\Delta T_{\mathrm{YREC}} = 3.4$ Gyr compared to the MIST values). The YREC models differ from the others in that they are calibrated to red giants rather than the Sun, and seeing as HD 28185 is a close match for the Sun in most respects, it is perhaps unsurprising that the YREC models do not reproduce its parameters as well. Excluding the YREC models, the remaining solar-calibrated models agree well, with $\sigma_M = 0.007$ $M_\odot$ and $\sigma_T = 0.3$ Gyr. We then conservatively increase these values by 50 per cent, that is, $\sigma_M = 0.010$ $M_\odot$ and $\sigma_T = 0.5$ Gyr. Adding these uncertainties in quadrature to our existing values, we adopt final values of $M = 0.974 \pm 0.018$ $M_\odot$ and $T = 8.3 \pm 1.0$ Gyr for the mass and age of HD 28185. We report our adopted stellar parameters in Table 1. HD 28185 is therefore a metal-rich star that is slightly lower in mass than the Sun but also substantially older and, as a result, is larger in size ($R = 1.048 \pm 0.015$ $R_\odot$).

There is no evidence that HD 28185 has any stellar companions. Tokovinin & Lépine (2012) observed that UCAC4 399$-$005893 at a separation of 1600 arcsec has a similar proper motion to HD 28185, resulting in this pair being accessioned to the Washington Double Star Catalog (Mason et al. 2001) as WDS 04264$-$1033. However, already in Tokovinin & Lépine (2012), this pair has a very low probability of physical association ($P_{\mathrm{phys}} = 0.001$), and with the addition of the *Gaia* parallax it can now be determined that UCAC4 399$-$005893 lies at a distance of 107 pc (Bailer-Jones et al. 2021), hence far in the background to HD 28185. No star found in *Gaia* DR3 can be identified as companions to HD 28185 due to a lack of agreement in proper motion and distance. Additionally, adaptive optics imaging from Chauvin et al. (2006) excludes much of the possible parameter space for stellar companions down to separations of less than an arcsecond. HD 28185 therefore appears to be a single star.

4 METHOD

4.1 Data

We have collated RV data for HD 28185 from the published literature. A total of seven separate data sets for six instruments are represented in the RV data:

(i) 40 CORALIE RVs spanning $1999 - 2001$, the discovery data for HD 28185 b, are taken from Santos et al. (2001). These observations do not overlap temporally with any of the remaining data sets.

Table 3. Proper motions of HD 28185 from the HGCA (Brandt 2021).

Measurement		μ_α (mas yr^{-1})	μ_δ (mas yr^{-1})
Hipparcos	μ_H	$+82.967 \pm 0.923$	-58.736 ± 0.801
Gaia EDR3	μ_G	$+84.070 \pm 0.024$	-59.637 ± 0.021
Hipparcos–Gaia	μ_HG	$+84.181 \pm 0.024$	-59.529 ± 0.019

(ii) 16 MIKE RVs spanning $2002 - 2009$ are from Feng et al. (2022). Compared to the MIKE data published in Minniti et al. (2009), this includes one additional observation.

(iii) 34 HRS RVs spanning $2005 - 2007$ are taken from Wittenmyer et al. (2009). These observations were taken as part of a targeted survey of known planet hosts; after the conclusion of this survey, observations of HD 28185 were not continued (Bowler, private communication).

(iv) 34 HIRES RVs spanning $2004 - 2019$ were published in Rosenthal et al. (2021). Four of these observations precede the 2004 instrument upgrade, and we observe that these observations show a large offset compared to the post-upgrade RVs; we thus treat these as two separate data sets for our model. We additionally opt to take nightly medians of the RVs. This results in a final set of 25 (4 + 21) HIRES RVs.

(v) 29 PFS RVs spanning $2011 - 2022$ were published in Feng et al. (2022). We take nightly bins of this data, resulting in a reduced set of 22 RV observations.

(vi) Finally, a limited set of 10 RVs from the HARPS spectrograph (Mayor et al. 2003) spanning $2003 - 2004$ are available in the ESO science archive,[1] and have been published in re-reduced form by Trifonov et al. (2020). Of these, we omit one relatively low signal-to-noise RV (BJD = 2453263.9) as it is a significant ($> 5\sigma$) outlier compared to the remaining measurements. This results in a set of nine HARPS RVs used in this work.[2]

In summary, our adopted RV data for HD 28185 consist of 146 measurements spread across 7 separate data sets, with a first-to-last time duration of 22.3 yr.

The astrometric data used in this work come from the *Hipparcos–Gaia* Catalog of Accelerations (HGCA; Brandt 2021). We refer the reader to Brandt (2018, 2021) and further to Brandt, Dupuy & Bowler (2019) for a full description of this data, but as a brief summary, the astrometric data in the HGCA consist of three *de facto* independent measurements of stellar proper motion; these are the *Hipparcos* proper motion (μ_H), here a linear combination of the original and new *Hipparcos* reductions (Perryman et al. 1997; van Leeuwen 2007), measured at an approximate epoch of 1991.25; the *Gaia* proper motion (μ_G), here from *Gaia* EDR3 (Gaia Collaboration 2021), measured at approximately epoch 2016.0; and lastly the *Hipparcos–Gaia* mean proper motion (μ_HG), which is derived from the change in sky position measured by the instruments and is hence time-averaged between the two epochs.

We reproduce the astrometry of HD 28185 in the HGCA in Table 3. As is typical for this data, the *Hipparcos* proper astrometry has the largest uncertainties, but the *Gaia* and *Hipparcos–Gaia* proper

---

[1] https://archive.eso.org/wdb/wdb/adp/phase3_spectral/form?phase3_collection = HARPS

[2] We note that there are two additional HARPS observations from 2011 in the ESO archive, but these were collected under different instrument settings to the aforementioned observations and show a significant RV offset, rendering them impertinent to the present analysis. Furthermore, a rich set of HARPS RVs spanning $2018 - 2021$ can also be found in the ESO archive; however, we abstain from analysis of this data prior to its formal publication.

motions are highly precise (0.025 mas yr$^{-1} \approx 5$ m s^{-1} at the distance of HD 28185) and are therefore strongly sensitive to long-term deviations in the motion of this star. For HD 28185, the $\mu_\mathrm{G} - \mu_\mathrm{HG}$ proper motion anomaly is $(-0.111 \pm 0.034, -0.108 \pm 0.028$ mas yr$^{-1})$, a $> 4\sigma$ significant difference ($\chi^2 = 22.9$, Brandt 2021) equivalent to a net velocity change of ~ 30 m s^{-1}.

4.2 Model

4.2.1 Model 1

The primary model used in this work to fit the RVs and astrometry of HD 28185 is based on the one in Venner et al. (2021), and we refer to reader to that work for a detailed description of the method. In this model, we use 30 variable parameters to fit the data described in Section 4.1. Two reflect the stellar mass M_* and the parallax ϖ, which are assigned Gaussian priors equal to the values given in Table 1. Five define the orbit of HD 28185 b as required to fit the RVs, these being the orbital period P, the RV semi-amplitude K, the eccentricity e, and argument of periastron ω (parametrized as $\sqrt{e} \sin \omega$ and $\sqrt{e} \cos \omega$), and the time of periastron T_P. Seven parameters then describe the orbit of HD 28185 c, of which the first five are analogous to those previously listed for HD 28185 b and the remainder are the orbital inclination i and the longitude of node Ω as required to fit to the astrometry. Finally, there are two normalizing terms for the proper motion of the system barycentre ($\mu_{\alpha,\mathrm{bary}}$ and $\mu_{\delta,\mathrm{bary}}$), and a total of 14 parameters delineate the offsets and jitter terms necessary for each of the seven RV data sets.

Compared to previous iterations of this model (Venner et al. 2021, 2022), the main alterations made for this work concern the inclusion of a second companion in the fit. Here, we have made the explicit assumption that HD 28185 b does not contribute to the astrometry. The astrometric signal of HD 28185 b is expected to be relatively large (~ 0.15 mas following Sozzetti 2005, equation 6, assuming $m = m \sin i$), but as its orbital period is shorter that the ≈ 3-yr observing spans of *Hipparcos* and *Gaia* DR3 its reflex signal in the *Hipparcos–Gaia* astrometry will be averaged out and reduced in amplitude (Kervella et al. 2019). More critical, however, is the 1.06 yr orbital period of HD 28185 b; it is exceptionally difficult to detect orbits with $P \approx 1$ yr using astrometry because the reflex signal is liable to absorption by the parallax (compare the paucity of *Gaia* DR3 astrometric orbits with ≈ 1 yr periods in Halbwachs et al. 2023, fig. 3). This means that it is likely that the astrometric signal of HD 28185 b has already been attenuated or altogether removed from the *Hipparcos–Gaia* proper motions as a result of the processing of the component astrometric solutions.

We use the Markov Chain Monte Carlo (MCMC) sampler EMCEE (Foreman-Mackey et al. 2013), the explore the posterior parameter space. Sixty walkers were used to sample the model for 5×10^5 steps, with confirmation of convergence of the MCMC performed as in Venner et al. (2021). We then discarded the first half of the chain as burn-in and saved every 150th step to extract our final posteriors.

4.2.2 Model 2: ORVARA

To independently test the accuracy of the Model 1, we also perform a joint fit to the RVs and astrometry of HD 28185 using ORVARA (Brandt et al. 2021b). ORVARA is designed for fitting any combination of RV, imaging, and *Hipparcos–Gaia* astrometry data for stars with one or more orbiting companions, and has previously been used to jointly fit orbits of a number of exoplanets with data from RVs and *Hipparcos–Gaia* astrometry (e.g. Li et al. 2021).

A salient difference compared to Model 1 is that the formalism of ORVARA requires fitting of astrometric reflex signals for all companions; this means that HD 28185 b is fitted for in the *Hipparcos–Gaia* astrometry, and hence two additional terms for the orbital inclination i and longitude of node Ω for HD 28185 b are included in the model. However, as argued previously in Section 4.2.1, the astrometric signal of HD 28185 b is unlikely to be detectable. Fitting four variables to three measurements of proper motion also hampers convergence. As a simplistic intervention, we assign a prior on the mass of HD 28185 b forcing $m \approx m \sin i$ and then disregard its astrometric posteriors. This reduces the impact of HD 28185 b on the astrometric fit, but slight differences may still remain compared to Model 1.

For Model 2, we again use the data described in Section 4.1, however due to computational limitations we exclude the small HARPS and pre-upgrade HIRES RV data sets. We use the parallel-tempered MCMC sampler PTEMCEE (Vousden, Farr & Mandel 2016, 2021) to explore the parameter space. We use 100 walkers and 20 temperatures and sample the model for 2×10^5 steps, discarding the first quarter of the chain as burn-in and saving at every 50th step for the final posteriors.

5 RESULTS

The results of our two joint fits to the RVs and astrometry of HD 28185 are shown in Table 4. We describe the results of both models in turn below.

5.1 Results for Model 1

In Fig. 1, we present the RV half of our joint fit from Model 1. Beginning with the parameters of HD 28185 b, we recover a tightly constrained orbit from the RV data; the key observable parameters are $P = 385.92^{+0.06}_{-0.07}$ d, $K = 164.8 \pm 0.9 \mathrm{m\,s^{-1}}$, and $e = 0.063 \pm 0.004$. Though the proximity of the orbital period of HD 28185 b to one year ($P = 1.0566 \pm 0.0002$ yr) means that the entire orbit cannot be covered in any single season, the 22-yr timespan of the RV observations means that most of the planetary orbit has now been sampled as a result of the slow drift in the orbital phase that can be observed from Earth. In combination with our adopted stellar mass of $M = 0.974 \pm 0.018\,\mathrm{M_\odot}$, the observable parameters for HD 28185 b result in a super-Jovian minimum mass of $m \sin i = 5.85 \pm 0.08\,M_J$.

Along with the reflex signal from HD 28185 b, a long-term acceleration is clearly visible in Fig. 1. We note at this point that in the study of similar long-term RV signals a perennial concern is represented by solar-like magnetic cycles, which frequently act on time-scales of decades and can produce planet-like RV signals (e.g. Díaz et al. 2016; Endl et al. 2016). This can, however, be discarded as an explanation for this RV signal as the HIRES spectra show no significant variability in the S-index, a stellar activity proxy which is highly sensitive to magnetic cycles (Butler et al. 2017; Rosenthal et al. 2021). The long-term RV signal must therefore correspond to an outer companion, as has been inferred in previous publications.

Unfortunately, the orbit of this outer companion is not completely sampled by the extant RV observations. Furthermore, the fiducial RV minimum is covered only by the CORALIE data, which does not overlap with the remaining data sets; this means that the offset between CORALIE and the remaining RV data can be only loosely constrained when considered directly, and it is hence not possible to confidently distinguish the long-term acceleration from a quadratic trend from the RVs alone. Resolution of orbit of HD 28185 c therefore depends crucially on the astrometry.

In Fig. 2, we plot our fit to the *Hipparcos–Gaia* astrometry of HD 28185. As noted in Section 4.1, of the three proper motion measurements, the *Hipparcos* proper motion is too imprecise to significantly contribute to the fit. Almost all of the astrometric information therefore comes from the difference between the *Gaia* proper motion and the time-averaged *Hipparcos–Gaia* proper motion. Though the measured velocity change between these measurements is significant ($\sim$30 m s^{-1}, Section 4.1), this is small compared to the $\approx$100 m s^{-1} range of variability observed in the RVs; in other words, the *net* tangential velocity change over the astrometric timespan is smaller than the total RV change over the RV timespan. As the tangential velocity semi-amplitude is equivalent to $\frac{K}{\sin i}$ (i.e. $\geq K$; Venner et al. 2021), the total change in tangential velocity cannot be smaller than the corresponding change in RV; however, the net change can be smaller if the period is close to $\sim$ 25 yr interval between the *Hipparcos* and *Gaia* DR3 epochs, as the signal will be averaged out from the mean proper motion. and the *Hipparcos–Gaia* proper motion represents the integrated motion across in the $\sim$25 yr interval between the *Hipparcos* and *Gaia* DR3 epochs, We therefore infer that the only possible explanation for the comparatively small size of the net astrometric signal is that there was a reversal in acceleration before the beginning of RV observations (separate to the RV reversal around $\sim$2015 present in the HIRES and PFS data); this is in turn best explained by hypothesizing that HD 28185 c completed about one complete orbit in the $\sim$25 yr interval between *Hipparcos* and *Gaia* observations.

This hypothesis is strongly borne out by our joint fit, from which we measure a well-constrained orbital period of 9090^{+460}_{-390} d ($24.9^{+1.3}_{-1.1}$ yr) for HD 28185 c. With the period resolved, it is thus possible to confidently constrain K from the RV data ($53.3^{+5.1}_{-4.7}\mathrm{m\,s^{-1}}$). Additionally, though its precision is limited by the incompleteness of the RV coverage, we are able to constrain the orbital eccentricity with reasonably high confidence ($e = 0.15 \pm 0.04$). This results in a minimum mass of $m \sin i = 5.4^{+0.6}_{-0.5}\,M_J$ for HD 28185 c. Though the astrometric data allow us to constrain the orbital inclination of this outer companion, the interpretation of this is complicated by the existence of a degeneracy in i which is symmetric around 90°, that is, $i = 66^{+11}_{-9}°$ or $114^{+9}_{-11}°$. Similar degeneracies in orbital inclination have frequently been found in joint fits of *Hipparcos–Gaia* astrometry and RVs for exoplanets (e.g. Li et al. 2021; Xiao et al. 2023; Philipot et al. 2023b), and occur in the circumstance where the *Hipparcos* proper motion is not sufficiently precise to independently detect the predicted variation in stellar tangential motion. When this is the case, the amplitude of tangential motion can still be constrained from the difference between the *Gaia* and *Hipparcos–Gaia* proper motions, but as this constitutes only two measurements and the latter is not time-resolved, in this scenario it is not possible to uniquely solve for both i and the longitude of node Ω (i.e. the *direction* of motion is ambiguous between clockwise and anticlockwise).

We demonstrate this covariance between i_c and Ω_c as it occurs in our joint model in Fig. 3; meanwhile, in Fig. 2 this degeneracy manifests in the symmetry of the best-fitting solutions between the two planes of tangential motion. While we cannot uniquely solve for the orbital inclination of HD 28185 c, because the two modes are symmetric around 90° we can solve for the value of $\sin i$ ($0.91^{+0.06}_{-0.07}$). This therefore allows for a unique value for the true mass of $m = 6.0 \pm 0.6\,M_J$ for HD 28185 c. We therefore determine that HD 28185 c is a planet of super-Jovian mass.

Based on the fitted orbital periods and our adopted stellar mass of $M = 0.974 \pm 0.018\,\mathrm{M_\odot}$, we derive semimajor axes of 1.034 ± 0.006 and $8.50^{+0.29}_{-0.26}$ au for HD 28185 b and c, respectively. Combined with their modest eccentricities, the orbits of these two planets are
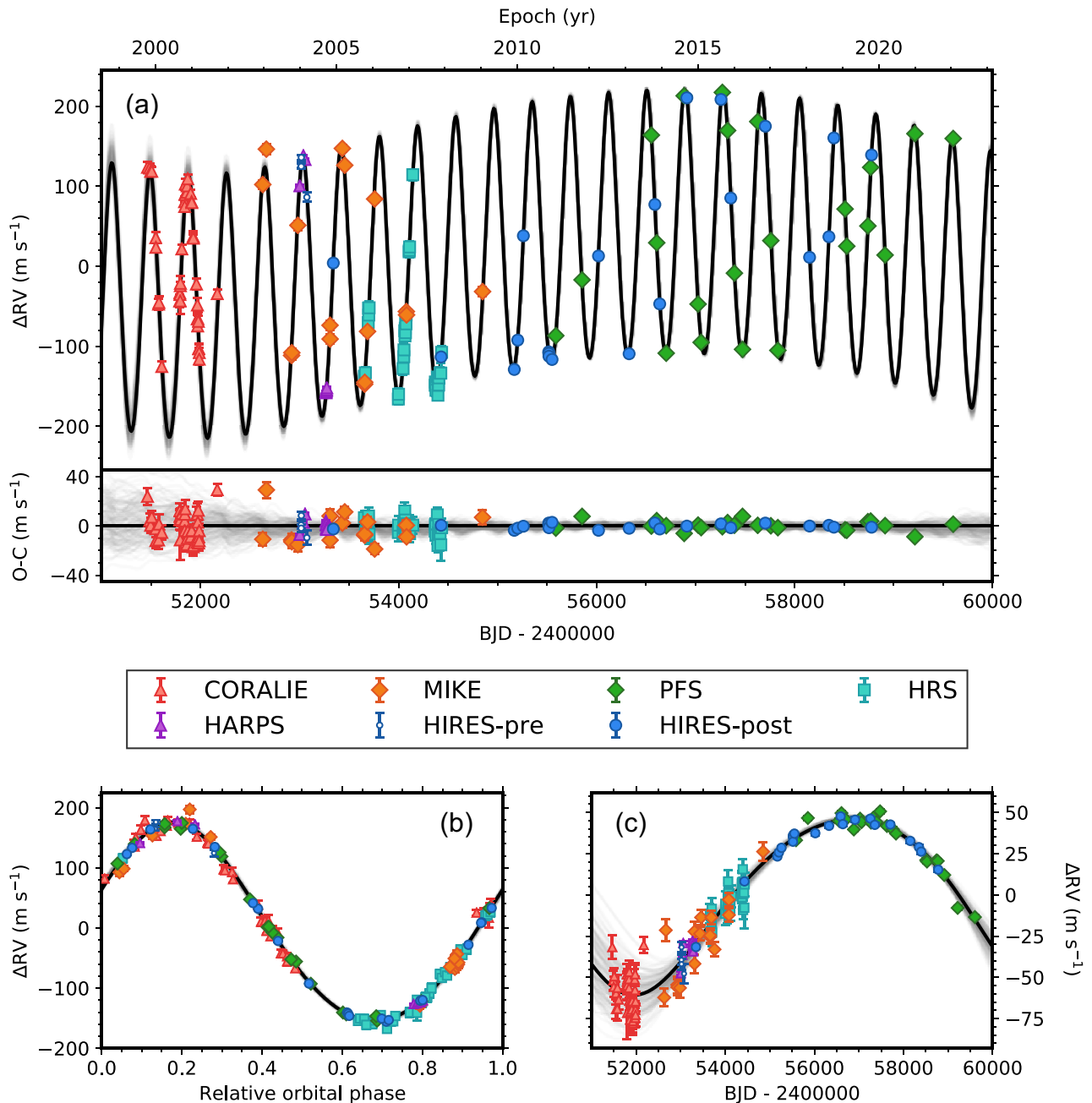
Figure 1. Our fit to the RV of HD 28185 from Model 1. Panel (a) shows the observed RVs over time; panel (b) shows the variation caused by HD 28185 b phase-folded to its orbital period, with the signal of HD 28185 c subtracted; and panel (c) shows the RV variation caused by HD 28185 c with HD 28185 b subtracted. Even with the combination of seven RV data sets from six different instruments, the orbit of HD 28185 c is not completely covered by the 22-yr timespan of the RVs; resolution of its orbit therefore depends crucially on the extension in observational duration offered by the astrometry (see Fig. 2).

comparable to those of Earth and Saturn among the Solar system planets. We return to further consider their properties in Section 6.

5.2 Results for Model 2

The results from Model 2 are in very good agreement with those from Model 1, so it will be sufficient to discuss these briefly.

All planetary parameters which can be compared between the models are consistent at the 1σ level. For the main observable parameters, we find $P_{\rm b} = 385.96 \pm 0.06$ d, $K_{\rm b} = 164.4 \pm 1.0 {\rm m\,s^{-1}}$, and $e_{\rm b} = 0.063 \pm 0.004$ for HD 28185 b and $P_{\rm c} = 9180^{+400}_{-340}$ d

$(25.1^{+1.1}_{-0.9}$ yr), $K_{\rm c} = 54.2^{+4.2}_{-4.0} {\rm m\,s^{-1}}$, and $e_{\rm c} = 0.14^{+0.04}_{-0.05}$ for HD 28185 c, all nearly identical to Model 1. The resulting semimajor axes for the two planets are 1.031 ± 0.006 and $8.52^{+0.25}_{-0.22}$ au and their minimum masses are 5.80 ± 0.08 $M_{\rm J}$ and 5.5 ± 0.4 $M_{\rm J}$, respectively.

Though the inclusion of HD 28185 b to the astrometric fit introduces a degree of 'fuzziness' to the relevant parameters for HD 28185 c, they still agree very well with Model 1. Bimodality for $i_{\rm c}$ and $\Omega_{\rm c}$ is less pronounced but we again find two main solutions, the first with $i = 71 \pm 12°$ and $\Omega = 270^{+30°}_{-35}$ and the second with $i = 109 \pm 12°$ and $\Omega = 187^{+32°}_{-33}$. The corresponding true mass of HD
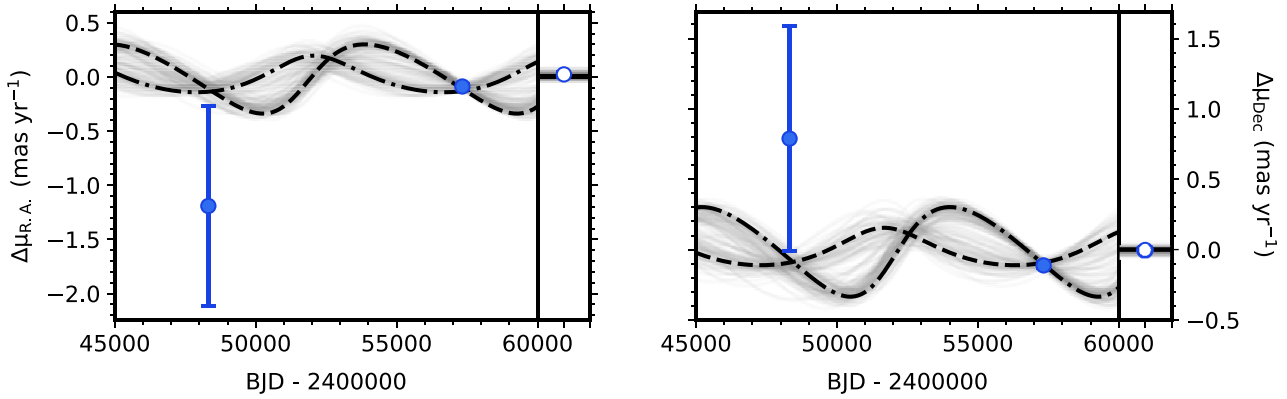
Figure 2. Our fit to the proper motion variability of HD 28185 caused by HD 28185 c from Model 1, in right ascension (left) and declination (right), normalized to the barycentre proper motion ($\mu_{\alpha,\text{bary}}$, $\mu_{\delta,\text{bary}}$). The two filled points in the main panels are the *Hipparcos* and *Gaia* proper motions, while the unfilled points in the side panels represent the *Hipparcos–Gaia* mean proper motions. The detection of HD 28185 c in the astrometry is driven by the highly precise *Gaia* and *Hipparcos–Gaia* proper motions; in concert with the RV data, the comparatively small net acceleration allows us to resolve the orbital period of HD 28185 c. However, due to the low precision of the *Hipparcos* proper motion there are two families of orbital solutions for HD 28185 c, represented by the dotted and dashed–dotted lines; see the text and Fig. 3 for elaboration.
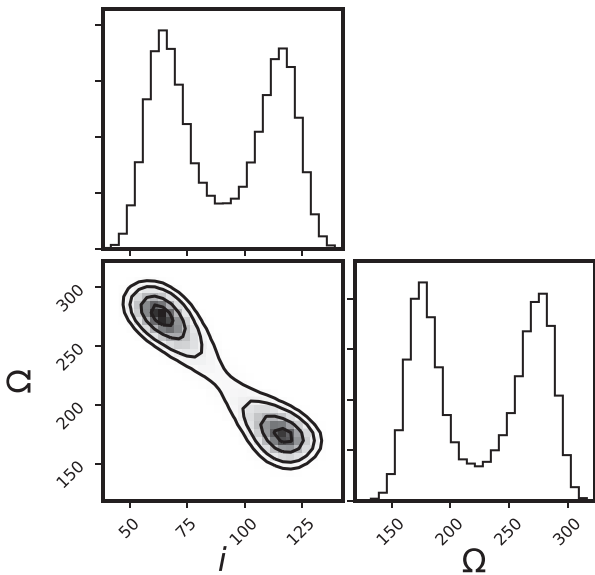

Figure 3. A CORNER plot (Foreman-Mackey 2016) of orbital inclination i versus longitude of node Ω for HD 28185 c. Due to limitations of the astrometric data, there are two peaks in the posterior which are mirrored around $i = 90°$, that is, $i = 66^{+11}_{-9}$° and $\Omega = 271^{+15}_{-21}$°, and $i = 114^{+9}_{-11}$° and $\Omega = 178^{+18}_{-14}$°.

28185 c is $m = 5.9^{+0.5}_{-0.4}$ M_J. All of these posteriors agree extremely well with Model 1.

The strong agreement between our two models supports the validity of our results. For the remainder of this work, we adopt the results from Model 1, but our interpretation would not change significantly if the results of Model 2 were used instead. Finally, we provide a selection of figures from Model 2 in Appendix A.

6 DISCUSSION

6.1 HD 28 185 b, the archetypal temperate Jupiter

At the time of its discovery HD 28185 b was the first known exoplanet with an Earth-like orbit, with $P = 383 \pm 2$ d, $e = 0.07 \pm 0.04$, and

$m \sin i = 5.7$ M_J (Santos et al. 2001). This original characterisation of HD 28185 b has been resoundingly confirmed through the two subsequent decades of continued RV observations, as we summarize in Table 5 (and see further in Section 2). In this work, we continue this with a highly precise characterization of this planet's parameters, with $P = 385.92^{+0.06}_{-0.07}$ d, $e = 0.063 \pm 0.004$, and $m \sin i = 5.85 \pm 0.08$ M_J.

HD 28185 b is the archetype of a now-numerous class of temperate giant planets. RV surveys have find a 5 per cent − 10 per cent occurrence rate for giant planets at Earth-like orbital separations around solar-type stars (Wittenmyer et al. 2020; Fulton et al. 2021). This approximates the location of the circumstellar habitable zone, for which the occurrence of transiting giant planet candidates was found to be comparable by Hill et al. (2018).

6.2 HD 28 185 c

6.2.1 Comparison with previously published results

For the outer companion HD 28185 c, we recover key parameters of $P = 9090^{+460}_{-390}$ d, $e = 0.15 \pm 0.04$, and $m = 6.0 \pm 0.6$ M_J (a CORNER plot of all posteriors is shown in Appendix B). We compare our results with those from previous publications in Table 6. The parameters initially reported by Rosenthal et al. (2021) for HD 28185 c are imprecise; $a = 15.9^{+7.3}_{-5.1}$ au, $e = 0.26^{+0.12}_{-0.09}$, and $m \sin i = 40^{+43}_{-28}$ M_J. Our solution in this work stands in reasonable agreement with theirs considering these large uncertainties, with our solution benefiting from the inclusion of additional RVs and astrometry.

However, our parameters differ greatly from those previously published by Feng et al. (2022), necessitating further scrutiny. In Fig. 4, we compare our results to those of Feng et al. (2022) for the key observable parameters of HD 28185 c. There are large discrepancies for several of the parameters such as P (10σ) and K (14σ). Even in cases where our posteriors nominally agree, it is also the uncertainties reported by Feng et al. (2022) are consistently smaller than those found in this work. This contrasts with the good agreement with our alternative fit using ORVARA (Model 2, Section 5.2), and we are unable to reproduce the results of Feng et al. (2022) using either of our models.

We first examine whether differences in data can explain these differences between our results. For their fit to the HD 28185

Table 4. Posterior parameters for our two joint fits to the RVs and astrometry. All values are medians and 1σ confidence intervals.

Parameter	Model 1 (adopted)		Model 2	
	HD 28185 b	HD 28185 c	HD 28185 b	HD 28185 c
Period P (d)	$385.92^{+0.06}_{-0.07}$	9090^{+460}_{-390}	385.96 ± 0.06	9170^{+400}_{-330}
Period P (yr)	1.0566 ± 0.0002	$24.9^{+1.3}_{-1.1}$	1.0567 ± 0.0002	$25.1^{+1.1}_{-0.9}$
RV semi-amplitude K (m s^{-1})	164.8 ± 0.9	$53.3^{+5.1}_{-4.7}$	164.4 ± 1.0	$54.2^{+4.2}_{-4.0}$
Eccentricity e	0.063 ± 0.004	0.15 ± 0.04	0.063 ± 0.004	$0.14^{+0.04}_{-0.05}$
Argument of periastron ω (°)	355.1 ± 3.9	162 ± 8	354 ± 4	163^{+9}_{-8}
Time of periastron T_P (JD)	2451870.2 ± 4.5	2460790^{+350}_{-280}	2451869.0 ± 4.3	2460870^{+370}_{-290}
Minimum mass $m \sin i$ (M_J)	5.85 ± 0.08	$5.4^{+0.6}_{-0.5}$	5.80 ± 0.08	5.5 ± 0.4
Semimajor axis a (au)	1.034 ± 0.006	$8.50^{+0.29}_{-0.26}$	1.031 ± 0.006	$8.52^{+0.25}_{-0.22}$
Orbital inclination i (°)	–	66^{+11}_{-9} 114^{+9}_{-11}	–	71 ± 12 109 ± 12
Longitude of node Ω (°)	–	271^{+15}_{-21} 178^{+18}_{-14}	–	270^{+30}_{-35} 187^{+32}_{-33}
$\sin i$	–	$0.91^{+0.06}_{-0.07}$	–	$0.95^{+0.05}_{-0.09}$
Orbital velocity semi-amplitude $\frac{K}{\sin i}$ (m s^{-1})	–	$59.0^{+5.7}_{-5.2}$	–	$58.6^{+4.8}_{-4.3}$
Mass m (M_J)	–	6.0 ± 0.6	–	$5.9^{+0.5}_{-0.4}$
Barycentre RA P.M. $\mu_{\alpha,\mathrm{bary}}$ (mas yr^{-1})	$+84.172 \pm 0.026$		–	–
Barycentre Dec. P.M. $\mu_{\delta,\mathrm{bary}}$ (mas yr^{-1})	-59.534 ± 0.020		–	–
CORALIE RV offset (m s^{-1})	50305.9 ± 8.2		50311.5^a	
MIKE RV offset (m s^{-1})	$55.3^{+4.6}_{-4.9}$		54.8^a	
PFS RV offset (m s^{-1})	$-31.5^{+4.0}_{-4.2}$		-32.9^a	
HRS RV offset (m s^{-1})	$95.1^{+4.3}_{-4.4}$		93.3^a	
HARPS RV offset (m s^{-1})	$75.6^{+4.0}_{-4.3}$		–	
HIRES pre-upgrade RV offset (m s^{-1})	$-118.3^{+6.0}_{-6.6}$		–	
HIRES post-upgrade RV offset (m s^{-1})	$20.5^{+3.8}_{-4.1}$		18.8^a	
CORALIE RV jitter (m s^{-1})	$9.0^{+2.1}_{-1.8}$		$8.0^{+1.9}_{-1.7}$	
MIKE RV jitter (m s^{-1})	$12.2^{+3.4}_{-2.6}$		$12.3^{+3.4}_{-2.6}$	
PFS RV jitter (m s^{-1})	$4.1^{+1.0}_{-0.7}$		$4.2^{+1.0}_{-0.8}$	
HRS RV jitter (m s^{-1})	$1.8^{+1.7}_{-1.2}$		$0.0^{+0.4}_{-0.0}$	
HARPS RV jitter (m s^{-1})	$6.0^{+2.3}_{-1.6}$		–	
HIRES pre-upgrade RV jitter (m s^{-1})	$7.7^{+9.6}_{-4.2}$		–	
HIRES post-upgrade RV jitter (m s^{-1})	$2.2^{+0.7}_{-0.5}$		$2.3^{+0.7}_{-0.5}$	

Note.^{a} ORVARA normalizes over RV zero-points, so only the best-fitting values are reported (Brandt et al. 2021b).

Table 5. Comparison of published parameters for HD 28185 b.

Parameter	Santos et al. (2001)	Minniti et al. (2009)	Wittenmyer et al. (2009)	Feng et al. (2022)	This work (Model 1)
P (d)	383 ± 2	379 ± 2	385.9 ± 0.6	$385.528^{+0.044}_{-0.055}$	$385.92^{+0.06}_{-0.07}$
K (m s^{-1})	161 ± 11	163.5 ± 3	158.8 ± 4.2	$163.66^{+0.65}_{-0.53}$	164.8 ± 0.9
e	0.07 ± 0.04	0.05 ± 0.03	0.092 ± 0.019	$0.055^{+0.004}_{-0.003}$	0.063 ± 0.004
ω (deg)	351 ± 25	44 ± 2	351.9 ± 8.2	$356.60^{+3.50}_{-3.16}$	355.1 ± 3.9
$m \sin i$ (M_J)	5.7	6.7	5.59 ± 0.33	$5.84^{+0.51}_{-0.49}$	5.85 ± 0.08
a (au)	1.03	1.1	1.032 ± 0.019	–	1.034 ± 0.006

system, Feng et al. (2022) use RV data from HARPS, HIRES, MIKE, and PFS; in comparison to our model they do not use the published CORALIE and HRS RVs (Section 4.1). The omission of the CORALIE data may be significant, as only this RV data covers the RV minimum for HD 28185 c. However this is found to be of secondary importance by our model, as the orbital period of HD 28185 c is instead mainly constrained by the astrometry.

As in our work, Feng et al. (2022) use data from *Hipparcos* and *Gaia* (E)DR3 as the astrometric information for their model.

However, they fit to the astrometry in a different way to most authors, and it could be argued that this explains of the observed differences. Beginning with the parametrization in the *Hipparcos* and *Gaia* astrometric solutions in the form of positions and proper motions, Feng et al. (2022) fit directly to both whereas Brandt (2018) and Kervella et al. (2019) reparametrize the data by converting the positional difference between *Hipparcos* and *Gaia* into a time-averaged proper motion, and it is in this basis that most authors prefer to fit the astrometry (e.g. Brandt et al. 2019, 2021b; Xuan & Wyatt

Table 6. Parameter comparison for HD 28185 c.

Parameter	Rosenthal et al. (2021)	Feng et al. (2022)	Model 1 (adopted)	Model 2
P (d)	–	17418^{+293}_{-673}	9090^{+460}_{-390}	9180^{+400}_{-340}
a (au)	$15.9^{+7.3}_{-5.1}$	$13.18^{+0.52}_{-0.69}$	$8.50^{+0.29}_{-0.26}$	$8.52^{+0.25}_{-0.22}$
K (m s^{-1})	–	$130.46^{+3.49}_{-1.59}$	$53.3^{+5.1}_{-4.7}$	–
e	$0.26^{+0.12}_{-0.09}$	$0.120^{+0.021}_{-0.022}$	0.15 ± 0.04	$0.14^{+0.04}_{-0.05}$
ω (°)	–	$107.79^{+9.55}_{-3.53}$	162 ± 8	163^{+9}_{-8}
$m \sin i$ (M_J)	40^{+43}_{-28}	–	$5.4^{+0.6}_{-0.5}$	–
i (°)	–	$57.65^{+8.15}_{-5.75}$	$66^{+11}_{-9}{}^{a}$	71 ± 12^{a}
Ω (°)	–	$62.12^{14.71}_{-12.77}$	$271^{+15}_{-21}{}^{a}$	$270^{+30}_{-35}{}^{a}$
m (M_J)	–	$19.64^{+2.27}_{-2.14}$	6.0 ± 0.6	$5.9^{+0.5}_{-0.4}$

*Note .$^{a}i < 90°$ solution only, for comparison with Feng et al. (2022).
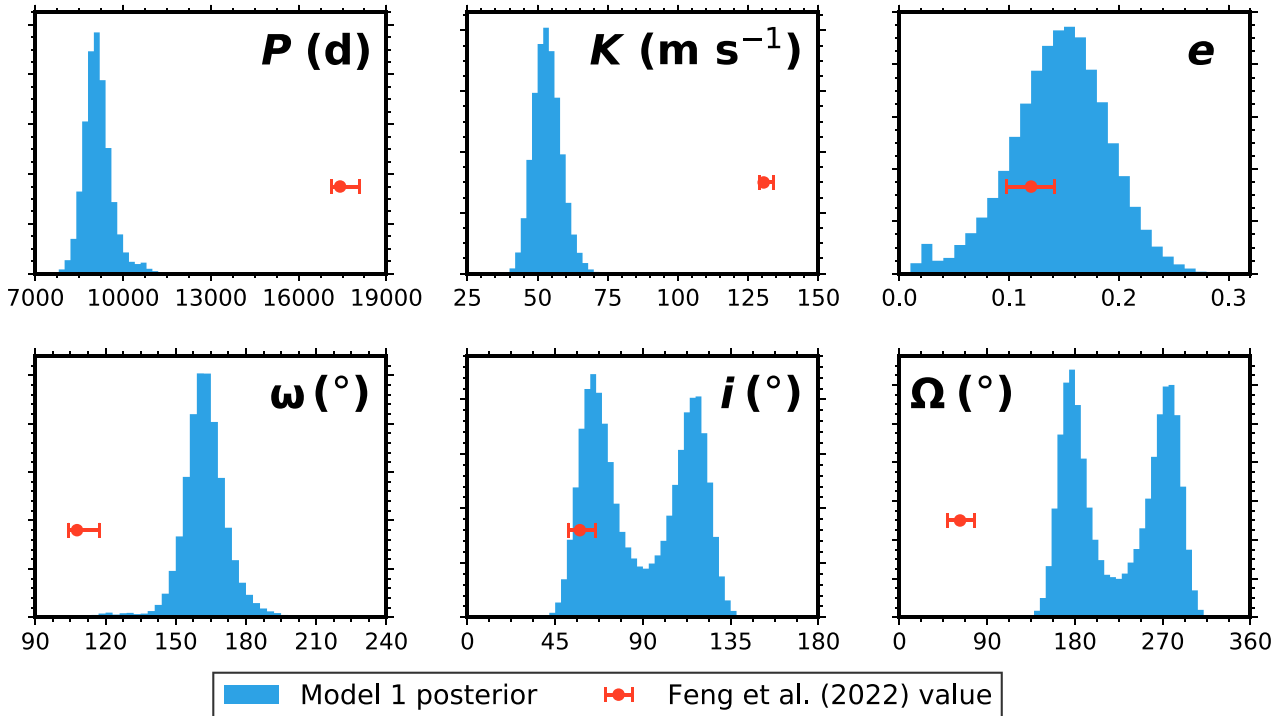

Figure 4. Comparison of our parameter posteriors for HD 28185 c from Model 1 (histograms) and values from Feng et al. (2022). Despite similar use of data many of the posteriors differ sharply between these two solutions, and even those parameters which are nominally compatible have confidence intervals of substantially different widths.

2020; Venner et al. 2021; Philipot et al. 2023a, b). Feng et al. (2022) recognize this and assert that their method is superior, claiming that conversion to proper motions is 'biased' without further elaboration (Feng et al. 2022, section 3).

To the contrary, however, the orbital information conveyed by the time-averaged proper motion is identical to that which can be gained directly from the positions (i.e. no information is lost in the reparametrization). This is because a single position measurement provides no information on the orbits of any companions, so it is the difference over time between the *Hipparcos* and *Gaia* positions that contains all of the relevant information (on this point see especially Kervella et al. 2019, section 3). The assertion that fitting to four position measurements is superior to fitting two time-averaged measurements in proper motion therefore does not

withstand scrutiny.[3] This difference in parametrization therefore cannot explain the observed discrepancies.

As our selections of RV and astrometry data are fundamentally similar, we postulate that the discrepancies between our results and those of Feng et al. (2022) are caused by differences between our methods and models. For HD 28185, it appears that their model does not reproduce the astrometry well. We have inspected their model figure for this system in Feng et al. (2022, appendix fig. 32), and observe that the *Gaia* proper motion lies approximately $(+0.35, +0.45)$

---

[3]This is claimed by Feng et al. (2022) in relation to Gliese 229 and 14 Herculis (on which see below). On the contrary, *Hipparcos–Gaia* astrometry is preferable as it includes secondary improvements such as a localized cross-calibration (Brandt 2018).

mas yr^{-1} from the model at the corresponding epoch. Considering the uncertainties listed in Table 3, this represents a $> 10\sigma$ discrepancy, and significantly contrasts with the good agreement between observations and model that we find in Fig. 2.

At this point, it becomes salient to note that HD 28185 is not the only system for which there are significant differences between Feng et al. (2022) and other studies. We cite a non-exhaustive selection of examples below:

(i) HD 38 529 has two massive planetary companions, of which the outer planet c has been detected with astrometry. Benedict et al. (2010) used *Hubble Space Telescope* (*HST*) astrometry to measure $i_c = 131.7 \pm 3.7°$ and $\Omega_c = 218.2 \pm 7.7°$.[4] Later, Xuan et al. (2020) used *Hipparcos–Gaia* astrometry for the same purpose and found $i_c = 135^{+8}_{-14}°$ and $\Omega_c = 217^{+15}_{-19}°$, in very good agreement with Benedict et al. (2010). However, based on similar data Feng et al. (2022) report $i_c = 104.56^{+6.39}_{-8.72}°$ and $\Omega_c = 37.8^{+16.23}_{-14.91}°$, which differ by 3.7σ and 11σ from the *HST* result, respectively.

(ii) 14 Herculis is a system with two long-period giant planets discovered with RVs. Bardalez Gagliuffi et al. (2021) used ORVARA to study the orbits of both planets; for the outer planet c, they found parameters including $P_c = 144^{+139}_{-58}$ yr, $e_c = 0.64^{+0.12}_{-0.13}$, $i_c = 101^{+31}_{-33}°$, and $m_c = 6.9^{+1.7}_{-1.0}$ M_J, while for planet b, the relevant parameter here is the orbital inclination $i_b = 32.7^{+5.3}_{-3.2}°$ which indicates a strong misalignment between the two orbits. Contrasting with these results, Feng et al. (2022) report parameters for 14 Her c of $P_c = 43.07^{+7.27}_{-5.19}$ yr, $e_c = 0.393^{+0.045}_{-0.048}$, $i_c = 129.10^{+6.26}_{-29.05}°$, and $m_c = 5.03^{+0.87}_{-1.07}$ M_J, while for planet b, they report similar RV parameters, but a strongly discordant orbital inclination of $i_b = 144.65^{+6.28}_{-3.24}°$ (25σ from Bardalez Gagliuffi et al. 2021). Most recently Benedict et al. (2023) have performed an independent fit incorporating *HST* astrometry, finding $P_c = 142.8 \pm 2.8$ yr, $e_c = 0.65 \pm 0.06$, $i_c = 82 \pm 14°$, $m_c = 7.1^{+1.0}_{-0.6}$ M_J, and $i_b = 36 \pm 3°$, which agree only with Bardalez Gagliuffi et al. (2021).

(iii) The star HD 62364 shows long-term RV variability in HARPS observations. Feng et al. (2022) fit this system with two long-period companions; $P_b = 75.02^{+9.78}_{-4.42}$ yr, $e_b = 0.863^{+0.012}_{-0.008}$, $m_b = 17.44^{+1.62}_{-1.67}$ M_J, and $P_c = 204.90^{+22.66}_{-18.79}$ yr, $e_c = 0.773 \pm 0.009$, $m_c = 24.93^{+2.68}_{-2.92}$ M_J. This is difficult to understand as the data can be much more simply explained by a single companion with parameters of $P = 14.15 \pm 0.06$ yr, $e = 0.6092 \pm 0.0042$, and $m = 17.46^{+0.62}_{-0.59}$ M_J, and there is no need to assume a second companion in the data (Xiao et al. 2023; also Frensch et al. 2023; Philipot et al. 2023b).

(iv) Gliese 229 B was one of the first brown dwarfs to be discovered. Based on RVs, imaging, and astrometry from the DR2 HGCA, Brandt et al. (2020) reported the first dynamical mass of 70 ± 5 M_J for this brown dwarf. Later, with additional data and updated astrometry from the EDR3 HGCA, Brandt et al. (2021c) used ORVARA to measure an updated and more precise mass of 71.4 ± 0.6 M_J for Gliese 229 B. However, based on largely the same data, Feng et al. (2022) report $m = 60.4^{+2.3}_{-2.4}$ M_J (4.6σ lower). It is not possible to reconcile this mass with ORVARA results (Brandt, private communication).

(v) HD 211847 was found to have a candidate brown dwarf companion from CORALIE RVs by Sahlmann et al. (2011). However, this companion was subsequently resolved in imaging observations

by Moutou et al. (2017), identifying HD 211847 B as an M-dwarf observed at a near-polar orbital inclination. Seemingly unaware of this result, Feng et al. (2022) claim that HD 211 847 B is a brown dwarf at $a = 4.51^{+0.29}_{-0.46}$ au with $m = 55.32^{+1.34}_{-18.49}$ M_J. This disagrees sharply with Xiao et al. (2023) and Philipot et al. (2023a), who incorporate the imaging detection into their fits and find $a = (6.83 \pm 0.06, 6.78 \pm 0.08)$ au and $m = \left(148.6^{+3.7}_{-3.6}, 148 \pm 5\right)$ M_J, respectively. The latter values for the mass agree with the photometric estimate of 155 ± 9 M_J (Moutou et al. 2017). The mass estimate of Feng et al. (2022) is therefore discrepant by 11σ, 24σ, and 18σ from the values of Moutou et al. (2017), Xiao et al. (2023), and Philipot et al. (2023a), respectively.

(vi) Gliese 680 and HD 111031 are two stars with RV accelerations for which Feng et al. (2022) claim brown dwarf companions with $a = \left(10.14^{+1.84}_{-1.70}, 13.10^{+0.75}_{-1.09}\right)$ au and $m = \left(25.10^{+6.16}_{-11.15}, 54.17^{+5.32}_{-6.15}\right)$ M_J, respectively. However, in both cases, these companions have previously been resolved as M-dwarfs in imaging observations (Ward-Duong et al. 2015; Gonzales et al. 2020; Dalba et al. 2021). Incorporating the imaging data into joint fits, Philipot et al. (2023b) find very different parameters of $a = \left(32^{+9}_{-6}, 21.1 \pm 0.6\right)$ au and $m = (186 \pm 4, 135 \pm 3)$ M_J, respectively. Feng et al. (2022) therefore underestimate the masses of these companions by 21σ and 13σ, respectively.

The above list is not exhaustive, but is sufficient to give an impression of the frequency and scope of disagreements between Feng et al. (2022) and other works. These go beyond any conceivable statistical explanation, as evidenced by the number of $> 10\sigma$ discrepancies listed above. These disagreements extend to many different works using many different fitting methods, chiefly based on *Hipparcos–Gaia* astrometry, but also including *HST* astrometry. It is also significant that for the systems where there are multiple independent sources of comparison such as 14 Her or HD 211847, the alternate solutions are mutually consistent with each other yet disagree with Feng et al. (2022); this is repeated by our two consistent sets of results for HD 28185. This demonstrates that the models causing this tension are those of Feng et al. (2022), rather than those of other authors.

It is not the case that all solutions from Feng et al. (2022) are inconsistent with results from other works; consider Xiao et al. (2023, section 6.2). However, the solutions showing the strongest discrepancies tend to be those longest orbital periods (typically $P > 10$ yr), which is also the case for HD 28185 c. This leads us to speculate that there is a period dependence in the origin of discrepant solutions in Feng et al. (2022). We intend to elaborate on this elsewhere (Venner et al., in preparation).

To conclude, we find that our solution for HD 28185 c differs significantly from that of Feng et al. (2022), and that this is paralleled by similar cases for other planets, brown dwarfs, and stars from the literature. Discrepancies chiefly occur for companions with comparatively long orbital periods, and the circumstances of these difficulties are sufficient to demonstrate that it is the solutions from Feng et al. (2022) which are in exception to other works rather than vice versa. This indicates that there is some issue with the method of Feng et al. (2022) which has resulted in inaccurate orbital solutions.[5]

---

[4]We have applied the angular rotation described by Xuan et al. (2020) to these values. Though the formalism of Xuan & Wyatt (2020) and Xuan et al. (2020) differ in the sign of ω from most works, for i and Ω they are consistent (Venner et al. 2021), so the comparison employed here is fair.

[5]This may explain the observation of Benedict et al. (2023) that the inclination distribution from Feng et al. (2022) does not match the distribution expected for random viewing orientations.
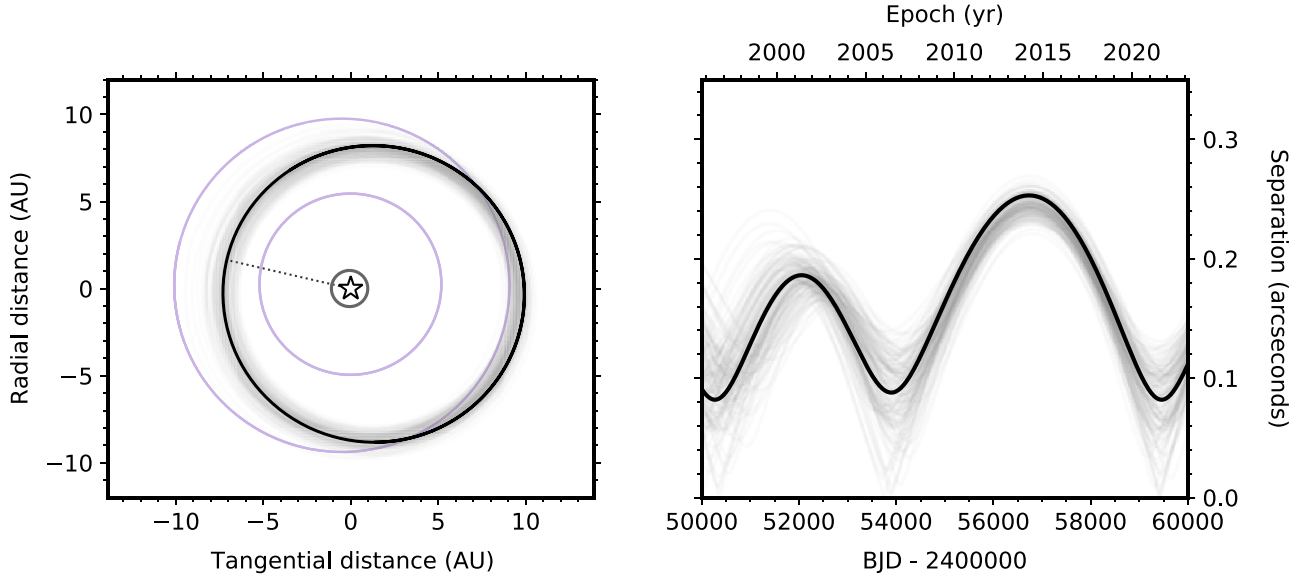
Figure 5. Left: plan view of the orbit of HD 28185 c. For comparison, we plot the orbits of Jupiter and Saturn. The orbit of HD 28185 b is also shown to scale; the planetary orbits are assumed to be coplanar. With $a = 8.50^{+0.29}_{-0.26}$ au and $e = 0.15 \pm 0.04$, HD 28185 c has an orbit reminiscent of Saturn. Right: planet–star separation over the observed orbit of HD 28185 c. Though its semimajor axis is exceptionally large among indirectly detected exoplanets, the age and distance of HD 28185 c means that it is too faint and too close to its star to be detected with modern imaging instruments. However, it is a potential target for imaging with future 30-m telescopes.

6.2.2 HD 28 185 c as a massive Saturn analogue

HD 28185 c is a significant addition to the sample of long-period exoplanets. At $P = 9090^{+460}_{-390}$ d (24.9$^{+1.3}_{-1.1}$ yr), HD 28185 c has among the longest orbital period of any exoplanet for which this parameter has been precisely constrained; furthermore, with $8.50^{+0.29}_{-0.26}$ au and $e = 0.15 \pm 0.04$, the orbit of this planet invites comparisons to Saturn ($P = 29.45$ yr; $a = 9.58$ au; and $e = 0.057$). However, its mass of 6.0 ± 0.6 M_J is larger than that of Saturn by a factor of 20. Like the inner planet b, HD 28185 c is therefore a 'Super-Jupiter.'

In Fig. 5, we visualize the orbit of HD 28185 c with comparison to the orbits of Jupiter and Saturn in the Solar system, along with the interior orbit of HD 28185 b. Though the orbit of HD 28185 c is somewhat smaller in scale than that of Saturn at apoastron their separations are approximately equal, and the exoplanet never reaches interior to the orbit of Jupiter ($a = 5.20$ au). HD 28185 c is therefore very much a massive analogue of Saturn.

We next place HD 28185 c in the context of the known long-period giant planets. We assemble the sample of exoplanets with well-constrained orbits with periods beyond $P > 5500$ d (≈ 15 yr), with this cut-off corresponding approximately to half the orbital period of Saturn. This effectively circumscribes the known exoplanets with periods substantially longer than that of Jupiter ($P = 11.86$ yr). A total of 37 exoplanets pass our selection, and we summarize their properties in Appendix C. Despite the difficulty inherent to the detection of these long-period planets, a majority were originally detected with RVs; in turn a majority of these planets have been further characterized using *Hipparcos–Gaia* astrometry, testifying to the significant impact these data have had on the study of long-period giant planets in five years since its inception (Brandt 2018; Kervella et al. 2019). In contrast our requirement of well-constrained orbits excludes most of the exoplanets current known from direct imaging, leaving only those with relatively close orbits ($a < 30$ au) in this sample. None the less, it is notable that the period ranges of the directly- and indirectly-detected exoplanets increasingly overlap,

and it is particularly remarkable how the parameters of HD 28185 c bear resemblance to the famous direct imaging planets β Pictoris b (Lagrange et al. 2009, 2010; $P = 8864^{+118}_{-113}$ d, $e = 0.119 \pm 0.008$, and $m = 9.3^{+2.6}_{-2.5}$ M_J, Brandt et al. 2021a) and 51 Eridani b (Macintosh et al. 2015; $P = 9100^{+1100}_{-1500}$ d, $e = 0.57^{+0.08}_{-0.06}$, and $m = 3.1^{+0.5}_{-0.7}$ M_J, Dupuy, Brandt & Brandt 2022). The outer detection limits of RVs and the inner limits of direct imaging currently lie at ~ 10 au for the typical targets of these methods (Nielsen et al. 2019; Fulton et al. 2021; Vigan et al. 2021), so this highlights how these methods are increasingly sampling a complementary sample of planets at Saturn-like orbital separations.

The similarity between HD 28185 c and these famous direct imaging planets motivates consideration of this planet's viability for imaging. Unfortunately, this is significantly impeded by the great age of the system (8.3 ± 1.0 Gyr, Table 1) and the modest projected separation, which never extends further than ~ 0.25 arcsec (Fig. 5). Using the ATMO 2020 atmosphere models (Phillips et al. 2020), we estimate that HD 28185 c has an effective temperature of ~ 230 K and a H-band planet–star contrast of $\approx 10^{-8}$, which is considerably beyond the detection capabilities of current near-infrared imaging instruments. The issue of contrast decreases towards the mid-infrared as the contribution of planetary thermal emission increases, such that the contrast reaches $\approx 10^{-4}$ at 10 μm. However, the planet cannot plausibly be detected with the *JWST* Mid-Infrared Instrument (MIRI) as it is always interior to the coronagraph inner working angle ($0.3 - 0.5$ arcsec depending on the filter; Boccaletti et al. 2015).

The prospects for direct detection improve significantly once 30-m class telescope instruments are brought into consideration. Using the Mid-infrared ELT Imager and Spectrograph (METIS) instrument as an example, $\sim 10^{-8}$ contrast in L band (3.5 μm) and $\sim 10^{-6}$ contrast in M-band (4.8 μm) are intended (Brandl et al. 2014). We estimate the corresponding contrasts for our target to be $\approx 10^{-7}$ and $\approx 10^{-4}$, respectively. Thus, while HD 28185 c lies beyond the capabilities of current technology, it may be a suitable target for direct imaging with future 30-m class imaging instruments.
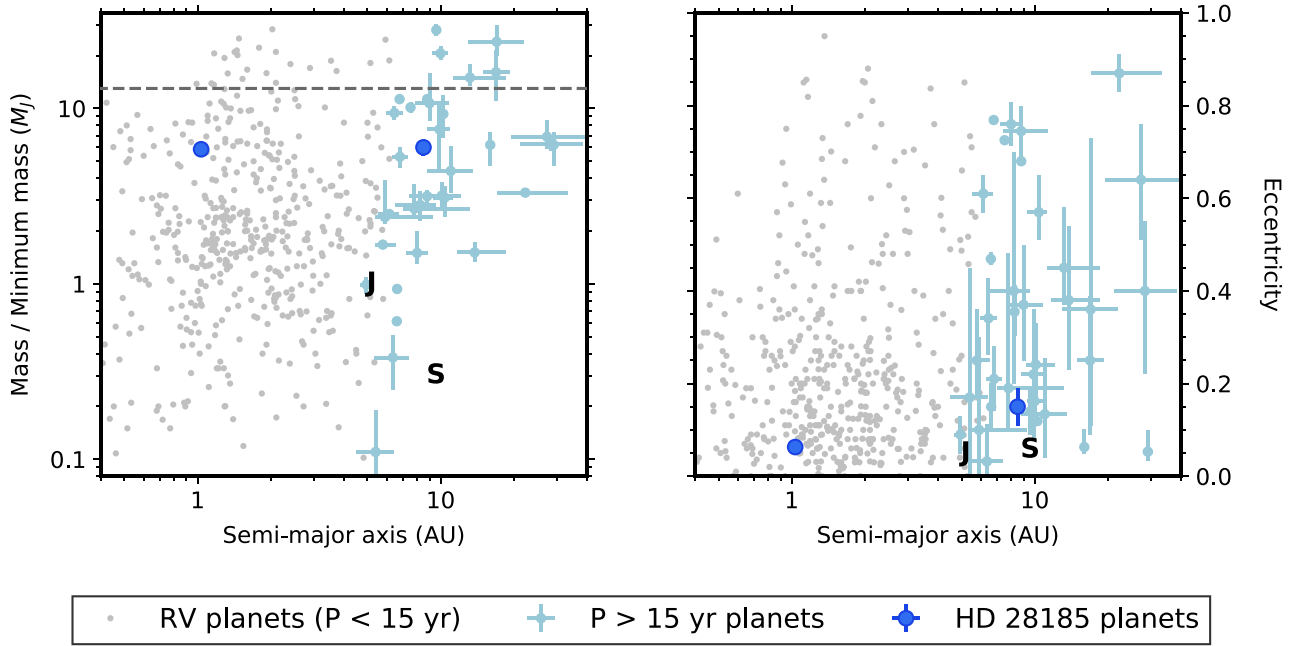
Figure 6. The HD 28185 planets placed in the context of known planets. Known long-period planets with $P > 15$ yr are highlighted, whereas shorter period planets from RV surveys are shown in grey (without error bars). We also label the locations of Jupiter and Saturn. Left: planet mass (or minimum mass) against semimajor axis; the location of the deuterium-burning limit, the traditional delimitation between planets and brown dwarfs, at 13 M_J is marked by the dotted line. Right: orbital eccentricity against semimajor axis. While HD 28185 b lies in a well-represented area of parameter space, HD 28185 c has only a small number of peers. It also has among the best-constrained parameters of any exoplanet in this region.

In Fig. 6, we elaborate on the context of the HD 28185 planets by plotting their mass and eccentricity against semimajor axis along with the long-period exoplanets selected in Appendix C, other shorter period exoplanets detected with RVs for specific comparison with HD 28185 b, and Jupiter and Saturn from the Solar system. As remarked in Section 6.1, HD 28185 b lies in a region of parameter space richly populated by Jovian planets with ≈1 au orbits. In contrast there is a comparatively small number of peers for HD 28185 c, undoubtedly reflecting the difficulty in the detection of exoplanets on such distant orbits. Though the total mass of the HD 28185 planetary system is relatively large ($\Sigma(m) \geq 12\ M_J$), HD 28185 b and c both retain low, Solar system-like orbital eccentricities; HD 28185 c in particular has one of the lowest eccentricities of any known exoplanet within its semimajor axis range, and contrasts with the substantial number of planets in the same region with $e \gtrsim 0.3$. This is indicative of a dynamically quiescent formation history for the HD 28185 system.

HD 28185 c is an important addition to the sample of long-period giant planets from RV surveys. The frequency of giant planets at such wide orbital separations is not yet well constrained; the addition of HD 28185 c to this group will help to constrain the occurrence rate of giant planets beyond the ice line, for which the occurrence rate function against orbital separation is not yet settled (Fernandes et al. 2019; Wittenmyer et al. 2020; Fulton et al. 2021; Lagrange et al. 2023). The discovery of other planets on similarly distant orbits with RVs, astrometry, and direct imaging will eventually lead to a complete picture of giant planet occurrence beyond the ice line.

7 CONCLUSIONS

HD 28185 is a Sun-like star found to have a giant planet on an Earth-like orbit by Santos et al. (2001), and suspected to have a more distant second companion since at least Chauvin et al. (2006). Recently, this outer companion has been claimed as a brown dwarf (Rosenthal

et al. 2021; Feng et al. 2022). In this work, we have revisited the companions of HD 28185 using published RV observations over a duration of 22 yr and *Hipparcos–Gaia* astrometry spanning 25 yr. We confirm the known properties of HD 28185 b with high precision, finding key parameters of $P_b = 385.92^{+0.06}_{-0.07}$ d, $e_b = 0.063 \pm 0.004$, and $m \sin i_b = 5.85 \pm 0.08\ M_J$, and identify this planet as the archetype of the now-numerous population of temperate Jovians. For the outer companion HD 28185 c, we find tightly constrained parameters of $P = 9090^{+460}_{-390}$ d ($24.9^{+1.3}_{-1.1}$ yr), $e = 0.15 \pm 0.04$, and $m = 6.0 \pm 0.6\ M_J$. We recover consistent results for this companion from two independent models, yet these values differ substantially from those found by Feng et al. (2022). In particular, our results are the first to return a planetary mass for HD 28185 c. We establish that this companion is a massive analogue of Saturn, having one of the longest orbital periods of any exoplanet found with indirect detection techniques. We highlight strong discrepancies between orbital solutions from Feng et al. (2022) and those of other works.

DATA AVAILABILITY

All data used in this work have been collated from publicly accessible depositories. The sources of the RVs and astrometry, which form the bulk of the data used in our analysis, are described in Section 4.1.

REFERENCES

Bailer-Jones C. A. L., Rybizki J., Fouesneau M., Demleitner M., Andrae R., 2021, AJ, 161, 147
Bardalez Gagliuffi D. C., Faherty J. K., Li Y., Brandt T. D., Williams L., Brandt G. M., Gelino C. R., 2021, ApJ, 922, L43
Benedict G. F., McArthur B. E., Bean J. L., Barnes R., Harrison T. E., Hatzes A., Martioli E., Nelan E. P., 2010, AJ, 139, 1844
Benedict G. F., McArthur B. E., Nelan E. P., Bean J. L., 2023, AJ, 166, 27
Bernstein R. et al., 2003, Proc. SPIE, 4841, 1694
Boccaletti A. et al., 2015, PASP, 127, 633
Brandl B. R. et al., 2014, Proc. SPIE, 9147, 914721
Brandt T. D., 2018, ApJS, 239, 31
Brandt T. D., 2021, ApJS, 254, 42
Brandt T. D., Dupuy T. J., Bowler B. P., 2019, AJ, 158, 140
Brandt T. D., Dupuy T. J., Bowler B. P., Bardalez Gagliuffi D. C., Faherty J., Brandt G. M., Michalik D., 2020, AJ, 160, 196
Brandt G. M., Brandt T. D., Dupuy T. J., Li Y., Michalik D., 2021a, AJ, 161, 179
Brandt T. D., Dupuy T. J., Li Y., Brandt G. M., Zeng Y., Michalik D., Bardalez Gagliuffi D. C., Raposo-Pulido V., 2021b, AJ, 162, 186
Brandt G. M. et al., 2021c, AJ, 162, 301
Brewer J. M., Fischer D. A., Valenti J. A., Piskunov N., 2016, ApJS, 225, 32
Butler R. P. et al., 2017, AJ, 153, 208
Chauvin G., Lagrange A. M., Udry S., Fusco T., Galland F., Naef D., Beuzit J. L., Mayor M., 2006, A&A, 456, 1165
Choi J., Dotter A., Conroy C., Cantiello M., Paxton B., Johnson B. D., 2016, ApJ, 823, 102
Crane J. D. et al., 2010, Proc. SPIE, 7735, 773553
Cumming A. et al., 2008, PASP, 120, 531
Currie T. et al., 2023, Science, 380, 198
Cutri R. M. et al., 2012, Explanatory Supplement to the WISE All-Sky Data Release Products
Dalba P. A. et al., 2021, AJ, 161, 123
de Beurs Z. L., de Wit J., Venner A., Berardo D., Bryan J., Winn J. N., Fulton B. J., Howard A. W., 2023, AJ, 166, 136
Díaz R. F. et al., 2016, A&A, 585, A134
Dotter A., 2016, ApJS, 222, 8
Dupuy T. J., Brandt G. M., Brandt T. D., 2022, MNRAS, 509, 4411
Endl M. et al., 2016, ApJ, 818, 34
Errico A. et al., 2022, AJ, 163, 273
Feng F. et al., 2022, ApJS, 262, 21
Fernandes R. B., Mulders G. D., Pascucci I., Mordasini C., Emsenhuber A., 2019, ApJ, 874, 81
Foreman-Mackey D., 2016, J. Open Source Softw., 1, 24
Foreman-Mackey D., Hogg D. W., Lang D., Goodman J., 2013, PASP, 125, 306
Franson K. et al., 2023, AJ, 165, 39
Frensch Y. G. C. et al., 2023, A&A, 675, A173
Fulton B. J. et al., 2021, ApJS, 255, 14
Gaia Collaboration, 2016, A&A, 595, A1
Gaia Collaboration 2021, A&A, 649, A1
Ghezzi L., Cunha K., Smith V. V., de Araújo F. X., Schuler S. C., de la Reza R., 2010, ApJ, 720, 1290
Gonzales E. J., Crepp J. R., Bechter E. B., Wood C. M., Johnson J. A., Montet B. T., Isaacson H., Howard A. W., 2020, ApJ, 893, 27
Gray R. O., Corbally C. J., Garrison R. F., McFadden M. T., Bubar E. J., McGahee C. E., O'Donoghue A. A., Knox E. R., 2006, AJ, 132, 161
Gregory P. C., Fischer D. A., 2010, MNRAS, 403, 731
Halbwachs J.-L. et al., 2023, A&A, 674, A9
Hill M. L., Kane S. R., Seperuelo Duarte E., Kopparapu R. K., Gelino D. M., Wittenmyer R. A., 2018, ApJ, 860, 67
Hinkley S. et al., 2023, A&A, 671, L5
Høg E. et al., 2000, A&A, 355, L27
Horner J. et al., 2019, AJ, 158, 100
Houk N., Swift C., 1999, Michigan Catalogue of Two-dimensional Spectral Types for the HD Stars. Vol. 5. Declinations -12.0 to 5.0. University of Michigan, Ann Arbor, MI
Kervella P., Arenou F., Mignard F., Thévenin F., 2019, A&A, 623, A72
Koposov S., 2021, segasai/minimint: Minimint 0.3.0. Zenodo, doi:10.5281/zenodo.5610692
Lagrange A. M. et al., 2009, A&A, 493, L21
Lagrange A. M. et al., 2010, Science, 329, 57
Lagrange A. M., Philipot F., Rubini P., Meunier N., Kiefer F., Kervella P., Delorme P., Beust H., 2023, A&A, 677, A71
Lenzen R. et al., 2003, Proc. SPIE, 4841, 944
Li Y. et al., 2021, AJ, 162, 266
Macintosh B. et al., 2015, Science, 350, 64
Maldonado J., Eiroa C., Villaver E., Montesinos B., Mora A., 2015, A&A, 579, A20
Mason B. D., Wycoff G. L., Hartkopf W. I., Douglass G. G., Worley C. E., 2001, AJ, 122, 3466
Matthews E. C. et al., 2024, Nature, 633, 789
Mayor M. et al., 2003, The Messenger, 114, 20
Minniti D., Butler R. P., López-Morales M., Shectman S. A., Adams F. C., Arriagada P., Boss A. P., Chambers J. E., 2009, ApJ, 693, 1424
Moutou C., Vigan A., Mesa D., Desidera S., Thébault P., Zurlo A., Salter G., 2017, A&A, 602, A87
Nielsen E. L. et al., 2019, AJ, 158, 13
Perryman M. A. C. et al., 1997, A&A, 500, 501
Philipot F., Lagrange A. M., Rubini P., Kiefer F., Chomez A., 2023a, A&A, 670, A65
Philipot F., Lagrange A. M., Kiefer F., Rubini P., Delorme P., Chomez A., 2023b, A&A, 678, A107
Phillips M. W. et al., 2020, A&A, 637, A38
Pinamonti M. et al., 2018, A&A, 617, A104
Pinamonti M. et al., 2023, A&A, 677, A122
Ramírez I., Meléndez J., Asplund M., 2014, A&A, 561, A7
Rickman E. L. et al., 2019, A&A, 625, A71
Rosenthal L. J. et al., 2021, ApJS, 255, 8
Sahlmann J. et al., 2011, A&A, 525, A95
Santos N. C., Mayor M., Naef D., Pepe F., Queloz D., Udry S., Burnet M., 2001, A&A, 379, 999
Santos N. C., Israelian G., Mayor M., 2004, A&A, 415, 1153
Sepulveda A. G., Bowler B. P., 2022, AJ, 163, 52
Skrutskie M. F. et al., 2006, AJ, 131, 1163
Soto M. G., Jenkins J. S., 2018, A&A, 615, A76
Sousa S. G. et al., 2008, A&A, 487, 373
Sozzetti A., 2005, PASP, 117, 1021
Tayar J., Claytor Z. R., Huber D., van Saders J., 2022, ApJ, 927, 31
Teske J. K., Shectman S. A., Vogt S. S., Díaz M., Butler R. P., Crane J. D., Thompson I. B., Arriagada P., 2016, AJ, 152, 167
Tokovinin A., Lépine S., 2012, AJ, 144, 102
Trifonov T., Tal-Or L., Zechmeister M., Kaminski A., Zucker S., Mazeh T., 2020, A&A, 636, A74
Tsantaki M., Sousa S. G., Adibekyan V. Z., Santos N. C., Mortier A., Israelian G., 2013, A&A, 555, A150
Tull R. G., 1998, Proc. SPIE, 3355, 387
Udry S. et al., 2000, A&A, 356, 590

van Leeuwen F., 2007, A&A, 474, 653

Venner A., Vanderburg A., Pearce L. A., 2021, AJ, 162, 12

Venner A., Pearce L. A., Vanderburg A., 2022, MNRAS, 516, 3431

Vigan A. et al., 2021, A&A, 651, A72

Vogt S. S. et al., 1994, Proc. SPIE, 2198, 362

Vogt S. S. et al., 2000, ApJ, 536, 902

Vogt S. S. et al., 2017, AJ, 154, 181

Vousden W. D., Farr W. M., Mandel I., 2016, MNRAS, 455, 1919

Vousden W., Farr W. M., Mandel I., 2021, Astrophysics Source Code Library, record ascl:2101.006

Ward-Duong K. et al., 2015, MNRAS, 449, 2618

Wittenmyer R. A., Endl M., Cochran W. D., Levison H. F., Henry G. W., 2009, ApJS, 182, 97

Wittenmyer R. A. et al., 2012, ApJ, 753, 169

Wittenmyer R. A. et al., 2017, AJ, 153, 167

Wittenmyer R. A. et al., 2020, MNRAS, 492, 377

Xiao G.-Y. et al., 2023, Res. Astron. Astrophys., 23, 055022

Xuan J. W., Wyatt M. C., 2020, MNRAS, 497, 2096

Xuan J. W., Kennedy G. M., Wyatt M. C., Yelverton B., 2020, MNRAS, 499, 5059

Zhang Z. et al., 2023, AJ, 166, 198

APPENDIX A: ORVARA FIGURES

In Fig. A1, we show plots from our ORVARA solution (Model 2, Section 5.2).
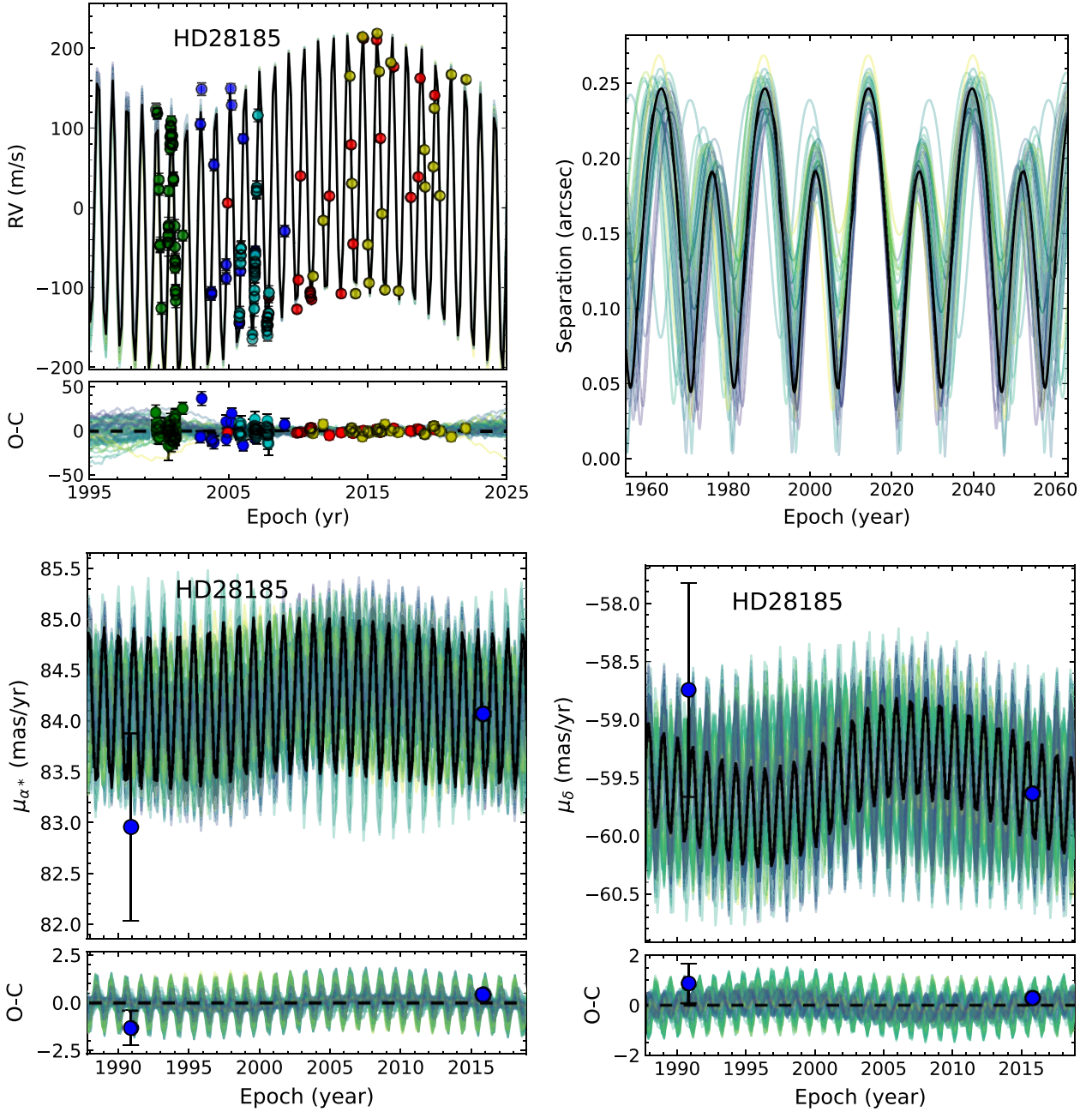
Figure A1. Figures from our ORVARA model (Model 2; see Section 5.2). Upper left: RVs; compare Fig. 1. Upper right: projected separation; compare Fig. 5. Lower left and lower right: *Hipparcos–Gaia* astrometry; compare Fig. 2, and observe that this differs in fitting for the astrometric signal of HD 28185 b.

APPENDIX B: CORNER FIGURE

In Fig. B1, we provide a CORNER plot for the modelled parameters of HD 28185 c from Model 1 (Section 5.1). This figure is a superset of Fig. 3, which includes only the orbital inclination i and longitude of node Ω.

Figure B1. CORNER plot (Foreman-Mackey 2016) of the posteriors for HD 28185 c.

APPENDIX C: COMPARATIVE LONG-PERIOD PLANET SAMPLE

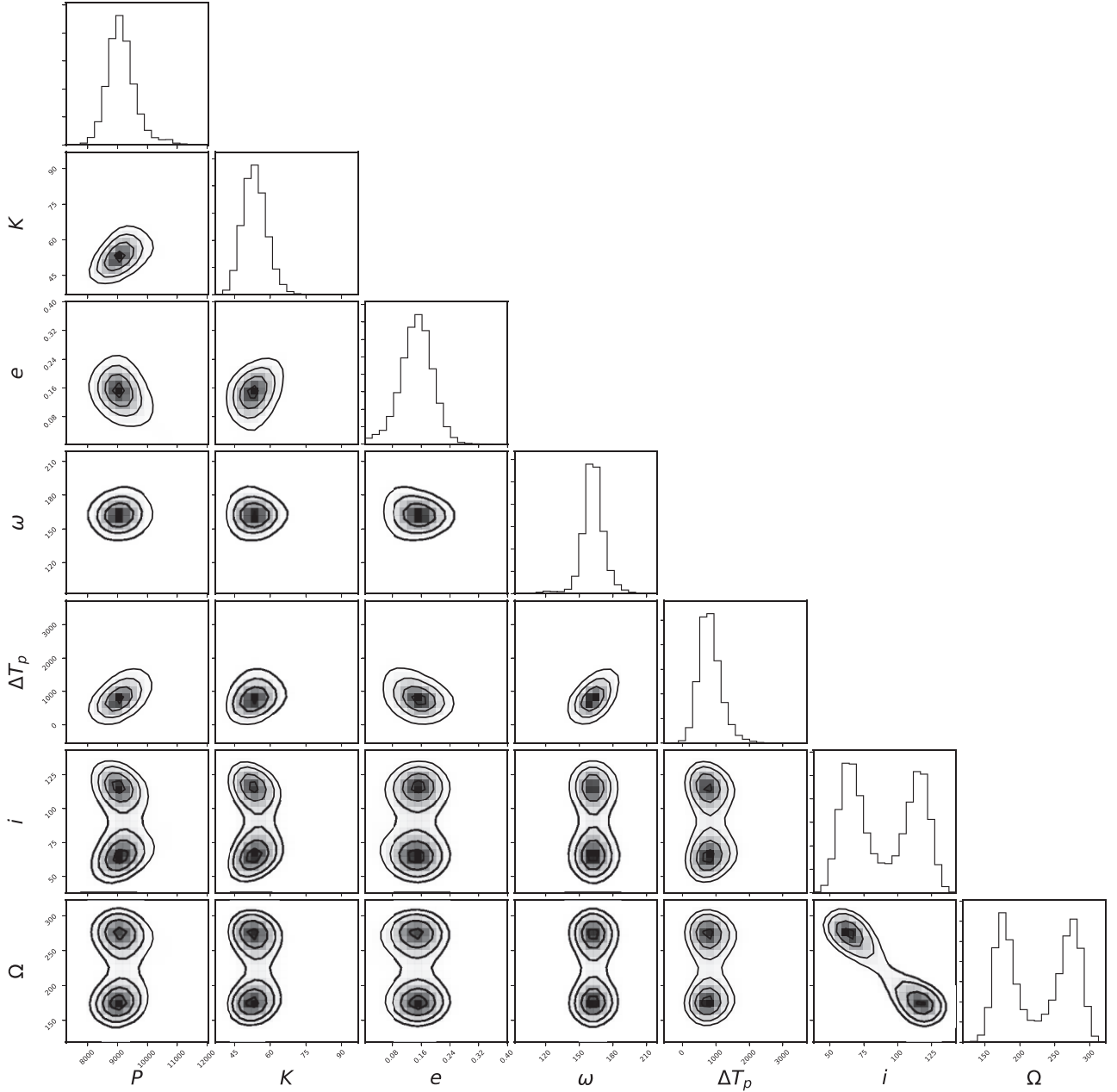In Table C7, we present the sample of long-period planets with well-constrained orbits used in Fig. 6. To assemble this list we began by querying the NASA Exoplanet Archive,[6] and then supplemented this with relevant literature results not present in the archive. For our selection, we restricted our sample to planets with $P > 5500$ d ($\approx$15 yr, or approximately half the orbital period of Saturn). We then manually excluded the planets with imprecise orbits identified as problematic by Lagrange et al. (2023), for example, HD 26161 b ($a = 20.4^{+7.9}_{-4.9}$ au, $m = 13.5^{+8.5}_{-3.7}$ M_J, Rosenthal et al. 2021; see Lagrange et al. 2023 for reservations on this target and other imprecise orbits). We also exclude certain spurious planets (Venner et al., in preparation). We also enforce an upper semimajor axis limit of $a < 30$ au for Fig. 6, though this makes little difference to the sample selection as there are very few planets with well-constrained orbits beyond this.

As mentioned in Section 6.2.2, 37 exoplanets pass this selection (including HD 28185 c). In Table C7, we list their names, orbital periods, semimajor axes, eccentricities, and masses, with a flag indicating whether the latter is a minimum mass ($m \sin i$). We then provide the reference for the quoted parameters and, in this case solely for the interest of the reader, a summary of the types of data used for the orbital solution in the 'Method' column.

---

[6] https://exoplanetarchive.ipac.caltech.edu/, accessed 2023 August 20.

Table C7. Long-period ($P > 5500$ d) exoplanet sample. HD 28185 c is highlighted in bold.

Name	Period (d)	a (au)	Eccentricity	Mass (M_J)	$m \sin i$?	Method	Reference
HD 34445 g	5700 ± 1500	6.36 ± 1.02	$0.032^{+0.08}_{-0.032}$	0.38 ± 0.13	Y	RV	Vogt et al. (2017)
HD 133131 B b	5769 ± 831	6.15 ± 0.59	0.61 ± 0.04	2.50 ± 0.05	Y	RV	Teske et al. (2016)
HD 134987 c	5960^{+170}_{-150}	$6.62^{+0.16}_{-0.15}$	0.15 ± 0.05	0.935 ± 0.06	Y	RV	Rosenthal et al. (2021)
Gliese 849 c	5990^{+110}_{-100}	$4.95^{+0.25}_{-0.28}$	0.09 ± 0.04	0.99 ± 0.11	Y	RV	Pinamonti et al. (2023)
HD 142 c	6005 ± 447	6.8 ± 0.5	0.21 ± 0.07	5.3 ± 0.7	Y	RV	Wittenmyer et al. (2012)
HD 219077 b	6199^{+52}_{-46}	6.78 ± 0.08	0.769 ± 0.002	11.3 ± 0.4		RV + HG	Philipot et al. (2023a) [a]
HIP 10337 c	6360^{+6260}_{-711}	$5.9^{+3.4}_{-0.5}$	$0.1^{+0.2}_{-0.1}$	$2.4^{+1.5}_{-0.2}$	Y	RV	Frensch et al. (2023)
HD 25015 b	6360^{+770}_{-690}	$6.45^{+0.52}_{-0.47}$	$0.341^{+0.086}_{-0.080}$	$9.42^{+0.85}_{-0.78}$		RV + HG	Xiao et al. (2023)
HD 181433 d	7012 ± 276	6.60 ± 0.22	0.469 ± 0.013	0.612 ± 0.004	Y	RV	Horner et al. (2019)
HD 4203 c	7400^{+8900}_{-1100}	$7.8^{+5.4}_{-0.8}$	$0.19^{+0.29}_{-0.09}$	$2.68^{+0.99}_{-0.24}$	Y	RV	Rosenthal et al. (2021)
HD 181234 b	7450^{+120}_{-100}	$7.52^{+0.16}_{-0.17}$	0.7254 ± 0.0094	$10.13^{+0.74}_{-0.63}$		RV + HG	Xiao et al. (2023)
Gliese 317 c	7500^{+1500}_{-720}	$5.78^{+0.75}_{-0.38}$	$0.25^{+0.11}_{-0.074}$	$1.673^{+0.078}_{-0.076}$	Y	RV	Rosenthal et al. (2021)
Gliese 15 A c	7600^{+2200}_{-1700}	$5.4^{+1.0}_{-0.9}$	$0.27^{+0.28}_{-0.19}$	$0.11^{+0.08}_{-0.06}$	Y	RV	Pinamonti et al. (2018)
AF Lep b	8150^{+2050}_{-2450}	$8.2^{+1.3}_{-1.7}$	$0.4^{+0.3}_{-0.2}$	$2.8^{+0.6}_{-0.5}$		Imaging + HG	Zhang et al. (2023)
HD 83443 c	8241^{+1019}_{-530}	8.0 ± 0.8	$0.760^{+0.046}_{-0.047}$	$1.5^{+0.5}_{-0.2}$		RV + HG	Errico et al. (2022)
HD 92788 c	8360^{+540}_{-390}	$8.26^{+0.36}_{-0.28}$	$0.355^{+0.057}_{-0.052}$	$2.81^{+0.18}_{-0.17}$	Y	RV	Rosenthal et al. (2021)
HAT-P$-$2 c	8500^{+2600}_{-1500}	$9.0^{+1.8}_{-1.1}$	$0.37^{+0.13}_{-0.12}$	$10.7^{+5.2}_{-2.2}$		RV + HG	de Beurs et al. (2023)
β Pic b	8864^{+118}_{-113}	10.26 ± 0.10	0.119 ± 0.008	$9.3^{+2.6}_{-2.5}$		Imaging + RV + HG	Brandt et al. (2021a)
HD 28185 c	9090^{+460}_{-390}	$8.50^{+0.29}_{-0.26}$	0.15 ± 0.04	6.0 ± 0.6		RV + HG	This work
51 Eri b	9100^{+1100}_{-1500}	$10.4^{+0.8}_{-1.1}$	$0.57^{+0.08}_{-0.06}$	$3.1^{+0.5}_{-0.7}$		Imaging + HG	Dupuy et al. (2022)
HD 206893 b	9350 ± 440	$9.6^{+0.4}_{-0.3}$	0.14 ± 0.05	$28.0^{+2.2}_{-2.1}$		Imaging + RV + HG	Hinkley et al. (2023)
HD 190984 b	9970^{+4380}_{-2200}	$8.8^{+2.5}_{-1.4}$	$0.745^{+0.054}_{-0.047}$	$3.16^{+0.25}_{-0.26}$		RV + HG	Xiao et al. (2023)
HD 221420 b	10120^{+1100}_{-910}	$9.99^{+0.74}_{-0.70}$	$0.162^{+0.035}_{-0.030}$	$20.6^{+2.0}_{-1.6}$		RV + HG	Li et al. (2021)
HD 16905 b	10256^{+618}_{-522}	$8.8^{+0.4}_{-0.3}$	$0.68^{+0.02}_{-0.01}$	$11.3^{+0.6}_{-0.7}$		RV + HG	Philipot et al. (2023b)
HD 50499 c	10400^{+3200}_{-1300}	$10.1^{+2.0}_{-0.9}$	$0.241^{+0.089}_{-0.075}$	$3.18^{+0.63}_{-0.46}$	Y	RV	Rosenthal et al. (2021)
HD 30177 c	11613 ± 1837	9.89 ± 1.04	0.22 ± 0.14	7.6 ± 3.1	Y	RV	Wittenmyer et al. (2017)
HD 73267 c	13900^{+5100}_{-4000}	$11.0^{+2.5}_{-2.2}$	$0.134^{+0.120}_{-0.095}$	$4.4^{+1.7}_{-1.1}$		RV + HG	Xiao et al. (2023)
HD 68988 c	16000^{-11000}_{-3500}	$13.2^{+5.3}_{-2.0}$	$0.45^{+0.13}_{-0.08}$	$15.0^{+2.8}_{-1.5}$	Y	RV	Rosenthal et al. (2021)
29 Cyg b	18600^{+6200}_{-2800}	$16.9^{+2.4}_{-1.9}$	$0.25^{+0.14}_{-0.16}$	$16.1^{+5.4}_{-5.0}$		Imaging + HG	Currie et al. (2023)
47 UMa d	19000^{+11000}_{-4000}	$13.8^{+4.8}_{-2.1}$	$0.38^{+0.16}_{-0.15}$	$1.51^{+0.22}_{-0.17}$	Y	RV	Rosenthal et al. (2021)
HR 8799 e	–	$16.0^{+0.5}_{-0.6}$	$0.063^{+0.037}_{-0.015}$	$6.2^{+1.1}_{-1.5}$ [b]		Imaging	Sepulveda & Bowler (2022)
HD 28736 b	22000^{+11000}_{-5800}	17^{+5}_{-4}	$0.36^{+0.37}_{-0.25}$	24^{+6}_{-4}		Imaging + RV + HG	Franson et al. (2023)
HD 111232 c	32100^{+13500}_{-9900}	$18.8^{+5.0}_{-4.1}$	$0.33^{+0.10}_{-0.09}$	$20.7^{+3.4}_{-3.2}$		RV + HG	Xiao et al. (2023)
HR 5183 b	37200^{+30700}_{-12400}	$22.3^{+11.0}_{-5.3}$	0.87 ± 0.04	$3.31^{+0.18}_{-0.14}$		RV + HG	Venner et al. (2022)
14 Her c	53000^{+51000}_{-21000}	$27.4^{+16}_{-7.9}$	$0.64^{+0.12}_{-0.13}$	$6.9^{+1.7}_{-1.0}$		RV + HG	Bardalez Gagliuffi et al. (2021)
ϵ Ind b	–	$28.4^{+10}_{-7.2}$	$0.40^{+0.15}_{-0.18}$	6.3 ± 0.6		Imaging + RV + HG	Matthews et al. (2024)
HR 8799 d	–	$29.2^{+1.3}_{-1.4}$	$0.053^{+0.047}_{-0.019}$	$6.2^{+1.1}_{-1.5}$ [b]		Imaging	Sepulveda & Bowler (2022)

Notes. [a] In Philipot et al. (2023a, table 3), P, a, and e for HD 219077 b appear to be switched with those of HD 211847 B. We use the values as attributed in the text.
[b] [Fe/H] $= 0.0$, normal mass prior solution from Sepulveda & Bowler (2022).

This paper has been typeset from a TEX/LATEX file prepared by the author.